SEDIMENTOLOGY

the journal of the
International Association of Sedimentologists

Clastic injectites, internal structures and flow regime during injection: the Sea Lion Injectite System, North Falkland Basin

Journal:	*Sedimentology*
Manuscript ID	SED-2018-OM-259.R2
Manuscript Type:	Original Manuscript
Date Submitted by the Author:	03-Sep-2019
Complete List of Authors:	Dodd, Thomas; British Geological Survey - Edinburgh Office; McCarthy, Dave; British Geological Survey - Edinburgh Office Clarke, Stuart; Keele University, Geography, Geology and the Environment
Keywords:	Clastic injectites, Internal structures, Ripple cross-lamination, Fluid connectivity, Deep-lacustrine, North Falkland Basin

Clastic injectites, internal structures and flow regime during injection: the Sea Lion Injectite System, North Falkland Basin

THOMAS J.H. DODD*[1&2], DAVE J. McCARTHY[1] and STUART M. CLARKE[2]

[1]*British Geological Survey, the Lyell Centre, Research Avenue South, Edinburgh, EH14 4AP, UK*, (E-mail: tdodd@bgs.ac.uk)

[2]*Basin Dynamics Research Group, School of Geography, Geology and Environment, Keele University, Keele, Staffordshire, ST55BG, UK*

ABSTRACT

This paper details and describes a suite of 143 sub-seismic-scale clastic injectites encountered within the early Cretaceous, early post-rift of the deep-lacustrine North Falkland Basin. The injectites, referred to here as the Sea Lion Injectite System (SLIS), are encountered below, above and in-between the hydrocarbon-bearing, deep-lacustrine turbidite sandstones of the Bleaker 15, Sea Lion North, Sea Lion, Casper and Beverley fans. Sedimentary structures are documented within the injectites including: planar laminations, mud-clast imbrication and clast alignment. Clasts align along cm-scale foresets formed through ripple-scale bedform migration in a hydraulically-open fracture. The style of flow within the injectite system is interpreted as initially through fluid turbulence during an open fracture phase, which was followed by a later stage where laminar flow dominated, most likely during the closing phase of the fracture system. The host rocks display evidence for ductile deformation, which along with ptygmatic folding of dykes and internally injected mud-clasts, suggests a period of injection into relatively uncompacted sediments. Evidence for brittle fracturing, in the form of stepped margins may be indicative of a separate phase of emplacement into more-compacted sediments. This variability in deformation styles is related to multi-phased injection episodes into host strata at different stages of consolidation and lithification at shallow burial depths. Injectites have been identified in four stratigraphic groupings: above the Bleaker 15 Fan and within/above the Sea Lion North Fan; within the hydrocarbon-bearing Sea Lion Fan; overlying the Sea Lion Fan; and above/below the hydrocarbon-bearing Casper and Beverley fans. This spatial association with the hydrocarbon-bearing fans of the North Falkland Basin is important, considering the ability of injectite networks to form effective fluid-flow conduits in the subsurface. Consequently, the findings of this study will improve the characterization of sub-seismic scale injectites (and therefore fluid conduits) within otherwise impermeable strata.

Keywords: Clastic injectites, Internal structures, Ripple cross-lamination, Fluid connectivity, Deep-lacustrine, North Falkland Basin

INTRODUCTION

Clastic injectites, also referred to as clastic dykes and sills, were first described by Murchison (1827) and have been widely recognised and described since the mid-1900s (Greensmith 1957; Peterson, 1968; Truswell, 1972; Hiscott, 1979; Dixon *et al*., 1995). They are considered as natural examples of hydraulic fracturing (Lorenz *et al*., 1991; Cosgrove, 2001; Jolly and Lonergan, 2002) because the process of their formation involves the pressure-driven injection of a fluid (a mix of clastic grains and water) into the surrounding material. In order for the injection to initiate, a pressure differential is required between, whereby the pore-fluid pressure exceeds the tensile strength of the host rock and the local confining stress oriented perpendicular to the fracture, causing fractures to initiate and propagate. Fracture propagation continues until the pressure dissipates, falling below the lithostatic pressure for sills, and below that of the minimum horizontal stress for the whole hydrofracture system (Jolly and Lonergan, 2002; Vigorito and Hurst, 2010).

Large-scale clastic injectites (*c.* 10–100 m in width) have been targeted for hydrocarbon exploration as remobilized sands can act as excellent hydrocarbon reservoirs (Hurst *et al*., 2005; Hurst and Cartwright, 2007; Szarawarksa *et al*., 2010); and their potential to act as fluid conduits within otherwise low-permeability strata is well documented (e.g. Hurst *et al*., 2003b; Jonk *et al*., 2003; Mazzini *et al*., 2003; Hurst *et al*., 2011). A number of publications have described the global distribution of injectites, at various scales (Huuse *et al*., 2010; Hurst *et al*., 2011, and references therein). The larger-scale structures have been well documented and described in terms of seismic-scale geometries (Hubbard *et al*., 2007; Vigorito and Hurst, 2010; Scott *et al*., 2013; Hurst and Vigorito, 2017).

The smaller scale features (*c.* 0.1 cm–10 m in width) can provide additional information concerning the sedimentary processes and flow rheology operating within fracture networks. Smaller scale injectites have been documented in core data (Duranti *et al.,* 2002; Duranti and Hurst, 2004; Hurst *et al.,* 2011 and references therein) and in outcrop (Rowe *et al.,* 2002; Hurst *et al.,* 2011 and references therein; Ravier *et al.,* 2015; Cobain *et al.,* 2015; 2017), where insights into their spatial, geometrical and sedimentological characteristics can be assessed.

Clastic injectites have been described in detail from outcrop in the Karoo Basin, South Africa (10s of cm wide dykes and up to 1.3 m thick sills; Cobain *et al*., 2015; 2017), where remobilized sand sourced from deep-water lobe deposits has intruded into overlying and underlying hemi-pelagic mudstones. In this example, a suite of structures was observed developed at the margins of injectites, including plumose ridges and ridged margins. Furthermore, excellent examples of clastic dyke and sill systems are also documented from the Aptian to Albian sedimentary fill of the Vocontian Basin, France (<0.5 m wide dykes and up to 6 m thick sills; Monnier *et al*., 2015; Ravier *et al*., 2015), the Hind Sandstone Member of the Carboniferous Craven Basin (<1 m wide dykes and up to 2 m thick sills; Kane, 2010), the upper Tortonian Marnoso-arenacea Formation, northern Italy (10–30 cm wide dykes; Gamberi, 2010), and the Cretaceous–Palaeocene Moreno Formation of the Panoche and Tumney Hills, California, USA (up to 18 m wide dykes; Vigorito *et al.,* 2008; Hurst *et al.,* 2011 and references therein; Scott *et al.*, 2013; Hurst and Vigorito, 2017).

In subsurface datasets, core penetrations offer laterally-limited, but useful snapshots into the style of intrusion and sedimentological characteristics of clastic injectites. They have been documented within core data from the North Sea (UKCS), including, the Alba and Penguin fields (Hurst and Cartwright, 2007;), the Tertiary reservoirs of the South Viking Graben (Jonk *et al*., 2005a), the Gryphon Field (Newman *et al*., 1993; Mazzini *et al*., 2003); the intra-Paleogene Hamsun Prospect, Norway (de Boer *et al.*, 2007); the Nini Field, Eastern North Sea (Svendsen *et al*., 2010), and the lower Palaeogene (Szarawarska *et al*., 2010). Injectites have been sparsely documented in lacustrine sedimentary basins, with examples from the Dinantian sediments of the Midland Valley of Scotland (Greensmith, 1957; Jonk *et al*., 2005b; Jonk *et al.,* 2007), the Eocene Green River Formation, Wyoming, USA (Töro and Pratt, 2015; 2016), and the Triassic strata of the Ordos Basin, central China (Gao *et al.*, 2019).

This work describes a series of clastic injectites that have been identified in conventional core data within, and in close proximity to, the Sea Lion Fan (and other fans) in the North Falkland Basin. Whilst the presence of these injectites has been mentioned briefly in the literature (Williams, 2015), they have not been described and documented in detail, or interpreted in terms of their probable genesis. A total of 143 sill and dyke-type injectites are identified within 455 m of conventional core data. Of the 143 injectites, 55 are discordant features, whilst 88 form concordant bodies. The injectites are observed both within and between deep-lacustrine turbidite fan deposits. Collectively, these injectites are referred to as the ‘Sea Lion Injectite System’ (SLIS), which describes all injectite features observed in the direct vicinity of the Sea Lion Fan, and includes those observed in overlying or adjacent depositional fan bodies. In documenting and describing the injectites of the SLIS, the following questions are addressed:

i.) Do sedimentary structures observed internally within the injectites of the SLIS reflect deposition by laminar or turbulent flow within the fracture network?

ii.) What is the character of the host rock during the emplacement of the SLIS?

iii.) What are the stratal relationships between the SLIS and the Sea Lion Fan (and other fans)?

iv.) What was the timing, injection depth and the primer/triggering mechanism?

v.) How might their presence impact fluid flow in the subsurface and associated hydrocarbon reservoir modelling?

Through this analysis, this study on sub-seismic-scale injectites adds not only to the general understanding of flow processes during injectite emplacement, but also to the relationships between injectites and the parent sands, and comments upon their potential to act as effective fluid conduits in the subsurface.

GEOLOGICAL SETTING

The North Falkland Basin, a Mesozoic-aged sedimentary basin located north of the Falkland Islands (Fig. 1), is a failed rift system comprising a series of offset depocentres following two dominant structural trends: north-south oriented faulting is predominant in the basin's northern area whilst significant NW-SE oriented faults control the south. The northern part of the basin has a half-graben geometry with the depocentre-controlling faults located on its eastern margin (Richards *et al.*, 1996a and 1996b; Richards and Fannin, 1997; Richards and Hillier, 2000a; Lohr and Underhill, 2015; Jones *et al.,* 2019). Rifting probably initiated in the the Jurassic period, and into the early Cretaceous, with some elements of the North Falkland Basin forming as a failed rift arm associated with the opening of the South Atlantic Ocean. The Eastern and Western grabens, which form the central rift system, are approximately 250 km long, from north to south, and 100 km wide from west to east, with a number of laterally-adjacent sub-basins that remain poorly understood (i.e. the Phyllis Graben; Fig. 1). Subsequently, the basin underwent a thermal sag phase that initiated during Berriasian–Valanginian times, forming the Transitional Unit (of Richards and Hillier, 2000a). This was followed by the deposition of a >1 km thick, early post-rift package, comprising the early Cretaceous-aged LC2–LC4 tectono-stratigraphical sub-units (as defined in Richards and Hillier, 2000a; Figs 2 and 3). The early post-rift is overlain by a thick middle post-rift unit (Richards and Hillier, 2000a), which forms a competent sealing lithology for the hydrocarbon system in the North Falkland Basin. It is within the LC3 sub-unit that the Sea Lion North, Sea Lion and Otter fans (Fig. 4A) were deposited along the eastern margin of the North Falkland Basin (Dodd *et al*., 2019), along with laterally adjacent turbidite systems of the Casper and Beverley fans (Bunt, 2015).

The Sea Lion Fan was first drilled by Rockhopper Exploration in 2010 and was declared as an oil discovery later that year (MacAulay, 2015). The Sea Lion Fan is composed of three lobes: Sea Lion 10 (SL10); Sea Lion 15 (SL15); and Sea Lion 20 (SL20). The lobes form a series of compensationally-offset stacked, tabular deposits (Figs 4B and 4C), that exhibit a complex suite of seismic amplitude architectures in plan view (as described in Dodd *et al*., 2019). Internally, the lobes comprise a series of high density turbidites, low density turbidites and hybrid event beds, interbedded within an otherwise hemi-limnic mudstone succession (Dodd *et al.,* 2019). This heterolithic succession, along with other fans and intervening mudstones in LC2 and LC3 (Bleaker 15, Sea Lion North, Casper and Beverley), were intruded into by a suite of clastic injectites that form the main focus of this study.

METHODS AND DATASETS

This study examines the relationship of 143 clastic injectites and their host strata from 455 m of non-oriented, vertically sliced, conventional core held as part of the Falkland Islands National Archive by the British Geological Survey. This dataset is supplemented by high-quality core photographs taken shortly after the 2010–2011 appraisal drilling of the Sea Lion Fan. During examination of the conventional core data and photographs, observations were made of injectite margin geometries, sedimentary structures and textures. These data have been augmented by a suite of high-quality down-hole wireline and sedimentary log data, which has been examined to determine the vertical and lateral spatial relationships between clastic injectites and the depositional sediments. Dyke and sill core plug porosity and permeability data have been provided (where available), which have been analysed, along with plotted dyke and sill geometrical information, in order to better assess potential impact of sub-seismic-scale injectites on hydrocarbon exploration and modelling.

Diagnostic features for clastic injectite identification

Diagnostic features can be split into three categories: the relationship of the injectite with host rocks (discordance); structures that formed externally, as impressions or erosional features within the host lithologies (Scott *et al*., 2009; Kane, 2010; Hurst *et al*., 2011; Cobain *et al*., 2015), which are challenging to identify at core scale; and structures that are formed internally within the injectite bodies during flow into the fracture. Ideally, a combination of these observations leads to a more accurate interpretation of sandstone bodies as either remobilized clastic injectites or sediments of primary deposition.

Host rock relationships

The presence of cross-cutting geometries, whereby sub-horizontal to vertical (>15–90°) features discordantly intersect primary bedding, is the most reliable method for identifying injectites. Alternative nomenclature has previously been used to describe intrusions at shallow angles, for example 'offshoots' (<25°; Truswell, 1972; Hiscott, 1979), or 'wings' (15–40°; Kane, 2010) that are more typically observed emanating from the edges of larger scale depositional sand bodies in seismic data (Hurst *et al.*, 2003a; Huuse *et al.,* 2007). In this study, any feature that ranges in dip between >15° and 90°, with respect to depositional bedding, is, for simplicity, termed a dyke.

Deformation of host rock lithologies can provide important information concerning emplacement timing, injection direction and characterization (*sensu* Kane, 2010; Ravier *et al.,* 2015). Injectite emplacement can affect host rock lithologies either through syn-intrusion deformation (Rowe *et al.,* 2002; Goździk and Van Loom, 2007; Ravier *et al.,* 2015), particularly during more ductile emplacement, or through post-intrusion differential compaction of mudstone in the host rock around the more competent sandstones (Hiscott, 1979; Kane, 2010).

Clastic sills are horizontal or slightly inclined (<15° relative to bedding) and are more challenging to identify than clastic dykes. One particular diagnostic feature of a clastic sill is stepped margins, or 'step-ramp-step' geometries (Cobain *et al.*, 2015). These geometries are observed at a range of scales, in a number of different settings, in both clastic intrusions (Duranti *et al.,* 2002; Vétel and Cartwright, 2010; Hurst *et al.,* 2011; Cobain *et al.*, 2015; Hurst and Vigorito, 2017) and igneous intrusions (Pollard *et al.*, 1975; Thomson and Hutton, 2004; Schofield *et al*., 2012). They form as the tips of intrusions become offset or segmented during propagation (Schofield *et al.*, 2012), resulting in sills that appear, in strike-section, to step up or down stratigraphy. Stepped margins, in-particular upper margins, with steep, regularly spaced steps, are unlikely to have formed through depositional sedimentary processes.

External features

Clastic injectites display a range of structures at their margins, including undulation crests (Kane, 2010), flute marks, grooves, rills, lobate-scours, frondescent marks and gutter marks

(Hurst *et al*., 2011 and references therein). In addition, they may have either smooth surfaces, blistered surfaces, plumose ridges or ridged margins (Cobain *et al*., 2015). This suite of margin structures, created as erosional features or impressions within the host rock, are observed typically at the outcrop-scale and can be extremely challenging to identify at core-scale.

Internal features

Internal features have been widely reported from examples of injectites, including: laminations; banding/layering/depositional layering; normal and reverse grading; aligned, sometimes imbricated, angular to rounded mud-clasts; ripple marks; and structureless (sandstone; 'Appendix A' in Hurst *et al*., 2011, and references therein). Laminations develop within clastic dykes (Hubbard *et al.*, 2007), often oriented parallel with margins, and are formed through the alignment and sorting of tabular grains within the sandstone (Peterson, 1968; Hannum, 1980; Taylor, 1982). Layering (Peterson, 1968), depositional layering (Hillier and Cosgrove, 2002), banding (horizontal, inclined and vertical; Scott *et al.,* 2009) or flow banding (Kane, 2010) is represented by multiple 'bands' of different grain sizes within a single dyke. Normal and reverse grading occurs either perpendicular to, or along the length of, dyke margins (Hurst *et al.*, 2011) and can form repeated bands (Peterson, 1968). Mud-clasts are commonly encountered within injectites, and are often aligned with dyke walls and sometimes display imbrication (Kawakami and Kawamura, 2002; Kane, 2010). There are only limited references to 'ripples' in clastic injectites (Smyers and Peterson, 1971; Van der Meer *et al.*, 2009; Phillips *et al.*, 2013). Despite the description of all these structures within the literature, a general absence of sedimentary structures (structureless) is the most common attribute found in remobilized sandstones (Hurst *et al*., 2003a; Hurst *et al.,* 2011 and references therein; Cobain *et al*., 2015).

Limitations of core data

The one-dimensional nature of subsurface core-data leads to difficulties in accurately distinguishing the genesis of bedding-concordant, structureless sandstone bodies. In particular, high-concentration sediment gravity flows, such as a high-density turbidity currents form thickly bedded, structureless sediments in deep-water environments (Lowe, 1979). These flows often deposit structureless, tabular sandstones, which are occasionally laminated and are normally graded. These depositional sandstones can appear almost identical to clastic sills formed through the intrusion of remobilized sand.

The identification of injectites around the Sea Lion Fan is further complicated by the limited number of wells that are cored. Furthermore, the vertical nature of 1D core data means that horizontal intrusions (sills) are more likely to be intersected than vertical features (dykes), particularly when the majority of dykes are thinner than that of the core barrel width. Finally, given the injectites are below the resolution of modern 3D seismic data (injectite maximum thicknesses of <70 cm, versus a seismic resolution of >12.5 m, at *c.* 2500 m TVDSS), it is challenging to characterize their distribution away from the cored well locations.

Despite these reservations and limitations, and taking into account the relatively small diameter of the core data (*c.* 12 cm), 143 injectites have been recognised in the 455 m of cored section. The relatively high intersection density (on average an injectite every three metres) may suggest that the injectites are laterally pervasive in the area around the Bleaker 15, Sea Lion North, Sea Lion, Casper and Beverley fans.

CLASTIC DYKES

Description

The clastic dykes in the SLIS comprise fine to medium-grained, sub-angular, well-sorted, quartz-rich, sandstones that form slightly inclined (>15° with respect to bedding) to vertical structures that cross-cut primary bedding (Fig. 5). The sandstones are variably cemented, with some examples displaying a pervasive cement (Fig. 5A), whilst others show visible porosity (Figs 5B and 5C) and oil-staining (Fig. 5D). The width of clastic dykes ranges from 0.3–11.2 cm, with a modal width of 2.5 cm. They extend vertically through the core, reaching heights of between 0.5–82.0 cm, with a modal height of 5 cm. They often appear feeding to, or from, clastic sills (Fig. 6). Margin geometries can be: smooth (Fig. 5A); cuspate with 'pod-like' lobate structures at varying scales (Fig. 5B); or jagged (Fig. 5C).

The dykes form a wide variety of contorted geometries, where sand thicknesses and the angle of discordance vary greatly (Figs 5A and 5B). The discordant bodies appear to plastically deform the host mudstones into which they are emplaced (Fig. 5B) and occasionally are observed alongside syn-sedimentary faulting or reverse displacements within host strata (Fig. 6B). In particular, primary depositional laminations within the host rocks are deformed in a ductile or plastic manner (Fig. 6), and are offset by, or around, the emplaced sand (Figs 5B and 6B).

A high proportion of the clastic dykes (57%) contain mud-clasts (Fig. 5) that typically have long-axis ranging between 0.5–5 cm and are angular, irregular or 'torn'/rhomboid in shape. The mud-clasts are typically sorted into similar-sized clast populations. Despite most mud-clasts ranging between 0.5–5 cm long there are a few examples of beds that contain much smaller clasts, ranging between 0.1–0.5 cm wide, forming a 'speckled texture' within the injectite (Fig. 5C; in this example the mud-clasts also display an alignment). Alignment is also observed in a number of other examples (Figs 5A, 5B and 5D), where elongate mud-clasts are oriented perpendicular or sub-perpendicular to the long-axis of the dyke margin.

Interpretation

The fine to medium-grade grain sizes are in keeping with grades known to preferentially-fluidize and re-mobilize (Lowe, 1975). The observation of clastic dykes feeding to, or from, clastic sills (Fig. 6), indicates a relationship between the two, suggesting they were coeval. The cross-cutting relationship between the dykes and the primary sedimentary bedding demonstrates that dyke emplacement occurred after the deposition of the lacustrine mudstones and turbidite sandstones (and therefore injection was not syn-depositional with those units).

The contorted geometries observed in some of the clastic dykes (Figs 5A and 5B) are interpreted as examples of ptygmatic folding (*sensu* Kuenen, 1968). Ptygmatic folding of clastic dykes has been associated with post-intrusion compaction of intruded host rocks, resulting in the compression of originally straight clastic dykes into folded structures (Hiscott, 1979; Duranti and Hurst, 2004; Parize *et al*., 2007). The necessity to first intrude the host rocks and then fold the clastic dykes through compaction implies that initial injection occurred into relatively uncompacted host rock (Kane, 2010). The ductile deformation of mudstone and tuff laminae (tonstein bands; Figs 5B and 6) provides additional support for this interpretation. The ptygmatic folding of dykes in the SLIS, along with ductile deformation observed in host rocks, is interpreted to have occurred whilst the host strata remained soft, only partially consolidated and therefore relatively uncompacted.

Injectite margins provide important information concerning wall-rock character, with lobate structures observed at cuspate margins (Figs 5B, 5C, 6A, 7D and 8C) interpreted as forming through ductile deformation in the host rock by the intruding sand body; these lobate or 'pod-like' features are unlikely to form in more brittle mediums. The presence of cuspate margins therefore suggests injection occurred into soft, unconsolidated and therefore mechanically weaker sediments. In contrast, smooth margins (Figs 5A and 5D) are interpreted as forming through injection into more brittle host rocks and jagged margins (Fig. 5C) simply reflect localised erosion along the host rock wall, which could be produced in either softer or more brittle host rocks.

The larger examples of mud-clasts (0.5–5 cm in width) entrained within the dykes were likely locally sourced, and eroded from the host rock of the injectite during emplacement (*cf.* Kawakami and Kawamura, 2002; Scott *et al.*, 2009; Ravier *et al.*, 2015). Evidence for localised erosion of the host rock in the SLIS is presented by jagged margins (Fig. 5C). The larger mud-clasts had limited transport potential from their sourcing host rock; significant transport distances in the fracture would otherwise progressively reduce their size through abrasion and fracturing processes in the flow (*sensu* Smith, 1972). By contrast, the smaller mud-clasts (0.1–0.5 cm) that form the 'speckled texture' (Fig. 5C; which are much smaller than the maximum dyke aperture), have extended transport potential away from the sourcing host-rock. Alternatively, the localised enrichment of small mud-clasts through corrasion processes acting on the host rock wall (*sensu* Scott *et al.*, 2013) is equally possible, although the similar sized mud-clast populations observed here may indicate at least some component of transport and sorting away from the host rock source. The possibility for the re-working of mud-clasts, which were originally part of the depositional sandstone, into the injectite system cannot be discounted.

The syn-sedimentary faulting or reverse displacements (shown in Fig. 5) represent small-scale examples of classical 'jack-up' structures formed during dyke emplacement (e.g. Huuse *et al.,* 2004; Szarawarska, 2010; Hurst *et al.,* 2016; Hurst and Vigorito, 2017). Collectively, these small-scale displacements may account for a potentially under-appreciated component of syn-intrusion deformation throughout an injectite network.

CLASTIC SILLS

Description

The clastic sills comprise fine to medium-grained, sub-angular, well-sorted, quartz-rich, homogeneous sandstones that are concordant with bedding (Figs 7, 8 and 9), with some contacts inclined by up to 15° relative to bedding. They are encountered in close proximity to clastic dykes, and are sometimes observed connected to these features (Fig. 6). The sandstones are variably cemented, with some examples displaying visible porosity and oil-staining (Figs 7A, 7D and 8), whereas others are pervasively cemented (Fig. 7B). Sill thicknesses range between 0.8–70 cm, with a modal thickness of 2 cm. They display a number of margin types, including stepped (Figs 7A, 7B, 7C and 8A), erosional (Figs 7D, 8D and 8E), flat (Figs 8B and 9) and cuspate (Fig. 7D). Sills often coincide (stratally) with light-grey and medium-brown tuffs (tonstein bands) within the otherwise dark-grey mudstone succession and, in many cases, intrude entirely within tuffs, often displaying erosional margins (Fig. 10C).

Mud-clasts are commonly observed within the sills (Figs 7D, 8 and 9), mostly ranging between 0.5–5 cm in length; some examples potentially reach >10 cm in length with their edges extending outside of the core barrel width (e.g. Figs 8A and 9). The mud-clasts generally display angular to sub-angular edges. They retain much of their original primary lamination, but often display an elongated or 'torn' texture, forming irregular, sometimes rhomboidal geometries (Figs 7D, 8B, 8C and 8E). In some examples, angular mud-clasts contain internal injections of sand with cuspate margins, which terminate abruptly at the edges of the clasts (Figs 8A, 8C 8D, 8E and 9B). The mud-clasts are lithologically identical to the surrounding host rocks, which are composed of hemi-limnic mudstones (as defined in Dodd *et al*., 2019).

Sorting of mud-clasts is present throughout, with the thin sills (1–10 cm thick) containing small mud-clasts (0.5–2.5 cm wide; Fig. 7D) and the thicker sills (>10 cm thick) containing larger mud-clasts (2.5–10 cm wide; Figs 9, 9A and 9B), with mud-clast sizes governed by maximum injectite aperture. A similar relationship has also been observed in sills from the Karoo Basin in South Africa (Cobain *et al.*, 2015). In some sills in this study mud-clasts are concentrated near to sill margins (Figs 7D and 9D).

There are numerous examples of mud-clast alignment within clastic sills. In some examples (Fig. 8) mud-clast alignment, mud-clast imbrication and structureless sandstones form a series of surfaces or 'sets' that are inclined relative to sill margins (Figs 8A and 8E), with set thicknesses approaching 8 cm in places. In these examples, mud-clast concentrations and maximum clast sizes display variation between individual sets (1–5 in Figs 8C and 8E), illustrating an element of mud-clasts sorting during deposition.

Planar laminations are also observed within sills (Figs 7A, 8A and 8B), highlighted by a range of aligned, millimetre-scale mud-clasts, tabular sand grains and occasionally instances of clay or silt-grade material. They are often observed concentrated at, and parallel to sill margins or slightly inclined, often joining-up to steps at the margins (Figs 8A and 8B). Other examples of planar laminations are observed in the centre of sills, otherwise composed of structureless sandstone (Fig. 7A). Despite the presence of structuring outlined in these examples, a high proportion (61%) of the clastic sills are composed of structureless sandstone.

Interpretation

The concordant bodies of well-sorted, fine to medium-grained sandstone represent clastic sills that formed through injection of fluidized sand along bedding planes. The fine to medium-grain sizes match those of grades known to preferentially-fluidize and re-mobilize (Lowe, 1975). The sills were fed by discordant clastic dyke systems that cross-cut primary bedding (Fig. 6). There is variability in the style of injection and the resultant deformation of host rocks, with stepped margins (Figs 7A, 7B and 7C) or flat margins (Fig. 8B) suggestive of brittle deformation. By contrast, cuspate margins indicate softer, more ductile deformation of host rocks (Fig. 7D). Erosional margins (Figs 7D, 8D and 8E) could form during either brittle or ductile intrusion events, the character of which would be reflected in the host rock wall morphology and of the resultant mud-clasts entrained within the flow.

Mud-clast geometries and distribution

The angular, irregular geometries of mud-clasts within the clastic sills (Figs 7D, 8 and 9B) offer some insights into the character of the host rock at the time of intrusion. The irregular geometries suggest that at least some of the mud-clasts were relatively soft at the time of erosion and entrainment into the fluidized sand. Elongate (Figs 7D and 8A), irregular and torn geometries (Fig. 8) likely formed through either shearing/stretching or as a consequence of squashing/compactional effects during transport (e.g. Jones and Rust, 1983; Pickering *et al.*, 1988). Additionally, their preserved geometries may have been further exaggerated during compaction and burial. In the opposite scenario where mud-clasts were brittle during transport, the thin, elongated and irregular forms would likely be broken during transport, making it difficult to preserve these geometries in the sill. The interpretation of relatively soft mud-clasts implies that at least some parts of the host rock, from which the mud-clasts were derived, was relatively soft and therefore only partially consolidated at the time of injection.

Furthermore, the examples of internal injectites, entirely contained within a single mud-clast, typically display cuspate margins, with lobate structures (Figs 8A, 8C, 8E and 9B; (some of which transcend the width of the core; Figs 8A and 9B), whilst the edge of those mud-clasts appear quite smooth or angular. The presence of cuspate margins in these examples is interpreted to suggest that at least one phase of emplacement of sand occurred within soft, relatively uncompacted host rock. However, in order to form the smooth or angular edges of those mud-clasts, the host-rock would need to be relatively competent at the time of erosion and entrainment into the fluidized sand. In order to produce these mud-clasts, at least two injection phases are required. The first phase intruded fluidized sand into soft, uncompacted host rock, forming the internal injectites, and a subsequent phase eroded the more-competent mud-clasts and deposited them within the clastic sill (Fig. 11). It might be possible to generate these geometries through a single, protracted injection phase, but this would require an element of syn-injection consolidation of the host rocks, something that could occur only during a period of rapid loading and burial.

In the two examples that transcend the core width (Figs 8A and 9B) an alternative model is that they are not clasts at all, but instead intruded host rock, with a network of smaller injectites connecting two separate sills above and below the mudstone interval. Whilst there is no unequivocal evidence to suggest or disprove either of these interpretations for these examples, figure 9C documents a mud-clast that has a very sharp boundary, across which there is an abrupt and clear grain size difference between the sand matrix of the sill (fine-grained) and the sand within the mud-clasts (very fine-grained; Fig. 9Bi). This would be extremely difficult to achieve through a single injection event as it would require a method for sorting of the grains across that zone. Finally, there is additional evidence for much smaller internally injected mud-clasts present in the system (Fig. 8E). This mud-clast displays the same internal injections, but has the advantage of being contained within the width of the core and is surrounded by a sand matrix; there is no question that this example is a mud-clast suspended in the sill and not intruded host rock. Together, these factors suggest that internally injected mud-clasts are present within the SLIS.

Mud-clast alignment, sorting and imbrication

The examples of inclined surfaces or sets of sorted, aligned, often imbricated mud-clasts (Figs 8 and 9B) are interpreted as having occurred along ripple foresets, forming ripple cross-lamination within the clastic sill. The foresets show variations in mud-clast concentrations and sizes (Figs 8C and 8E), indicating an element of sorting occurring during ripple migration within the injectite system. In these examples, the interpretation of the concordant sandstone beds as sills, rather than as depositional units, is supported by a clearly-defined stepped upper margin (Fig. 8A) and upper/lower erosional contacts, with associated feeder dykes and sills

(Fig. 8D). In most instances, the ripple cross-lamination forms along the lower margin of the sill, aggrading towards the centre, suggesting a relationship with the basal contact.

Similar inclined sets of mud-clasts and cleaner sandstone have been recognised by other workers, including: the 'oversteepened laminae' identified in figure 4 of Duranti and Hurst (2004); the differential flow and size differentiation of mud-clasts of Kawakami and Kawamura (2002); and, crude long-axis clast alignment and irregular low-angle laminae of de Boer et al. (2007). Furthermore, ripple structures have previously been recorded in injectites, including: ripple marks' of Smeyers and Peterson (1971); vertically oriented 'climbing ripple structures' in clastic dykes from a glacial setting (Van der Meer *et al.*, 2009); and 'ripple drift lamination' observed infilling subglacial hydrofactures (Phillips *et al.*, 2013). The importance of observing ripple migration within an injectite is that the fluid-sand mix would need to be sufficiently dilute (and therefore not concentrated) in order to permit ripple-scale bedforms to develop and migrate within the injectite network. This suggests the fluid-sediment mix during this time was not concentrated (and not cohesive/laminar flow) and therefore had the potential to be turbulent in character.

Planar laminations

The planar laminations observed within clastic sills of the SLIS (Figs 7A, 8A and 8B) can be attributed to two possible mechanisms of formation. Planar laminations within sills have previously been associated with periods of traction occurring within the fluid-sediment mix in a clastic sill (Kawakami and Kawamura, 2002; Scott *et al.*, 2009). The alternative method for generating laminations within a clastic sill is through the shearing of concentrated liquefied sand, deforming by hydroplastic laminar flow (Lowe, 1976; Allen, 1984; Hurst *et al.*, 2011). This style of flow may also lead to the generation of flow banding or layering within injectites (Peterson, 1968; Hillier and Cosgrove, 2002; Kane, 2010), and has also been associated with consolidation laminae (Archer, 1984). However, taken in isolation it is challenging to attribute any form of planar lamination to a single flow process as the sedimentary structure can be formed under a number of conditions.

In the SLIS, the planar laminations occur in two main groups: in the middle of sills (Fig. 7A); and at the top of sills (Figs 8A and 8B). In this interpretation, the laminae observed at the top of sills are attributed to more dilute, potentially turbulent flow, with the laminae forming near the top during flow deceleration and the onset of tractional processes. This is in contrast with laminae in the centre of the sills, particularly where they are surrounded by structureless sandstone (Fig. 7A), which are interpreted as forming through the shearing of concentrated fluid-sediment mixes and therefore associated with laminar flow (Fig. 11).

DISTRIBUTION OF INJECTITES

The potential role of injectites to form fluid conduits between otherwise disconnected reservoir bodies is of particular importance to the hydrocarbon industry (Hurst *et al*., 2003b; Jonk *et al.*, 2003; Mazzini *et al.*, 2003; Hurst *et al.*, 2011). Therefore, in the case of the hydrocarbon-bearing Sea Lion, Casper and Beverley fans, it is informative to evaluate the spatial distribution of the SLIS in relation to these depositional units. As the injectites of the SLIS are only identifiable in core data, caution must be exercised when considering the distribution of features in non-cored sections of wells. The injectites are separated into four, stratigraphically-significant groupings.

The stratigraphically lowest grouping of injectites occur above the Bleaker 15 Fan (B15) and within/above the overlying Sea Lion North Fan (SLN; Figs 2 and 3). The association is documented in well 14/10-3 (Figs 12 and 13), located to the north of the Sea Lion Field (Fig. 1). This grouping has an apparent dyke-dominance (29 dykes vs. 19 sills), corresponding with intervals comprising lacustrine mudstone within an otherwise sand-rich succession. The injectites between SLN and the underlying B15 were formed within the uppermost deposits of the LC2 sub-unit, whereas the examples within and above SLN are within LC3 sub-unit (Fig. 2 and 3; Richards and Hillier, 2000a).

The second grouping are within the overlying Sea Lion Fan (Figs 2, 3 and 4), where the injectites are observed within the SL15 lobe, in wells 14/10-4, 14/10-6 and 14/10-7 (Fig. 12), in the northern part of the Sea Lion Field (Fig. 1). To date, injectites are not intersected in SL10 or SL20 (Fig. 12), where the cored intervals are more sand-rich (Fig. 13). The injectites in SL15 have an apparent sill-dominance (3 dykes vs. 14 sills) and are associated with hemi-limnic mudstone intervals within the fan succession (Fig. 13).

The third grouping of injectites is within mudstone-prone successions overlying the Sea Lion Fan, chiefly above the SL10, in wells 14/10-9Z and 14/15-4Z (Figs 12 and 13). These wells are located on the western side of the Sea Lion Field (Fig. 1), intersecting the more distal parts of the Sea Lion Fan (Dodd *et al.*, 2019). These injectites occur in a dense accumulation between SL10 and the overlying Casper Fan, and like with SL15, have an apparent sill-dominance (17 dykes vs. 48 sills).

The final grouping of injectites are observed surrounding two fan bodies that overly the Sea Lion Fan: above the Casper Fan in 14/15-4Z; and two examples of dykes above the Beverley Fan in 14/15-4Z (Figs 2, 3 12 and 13).

Injectites are absent in core data from within the SL10 and SL20 lobes of the Sea Lion Fan in wells 14/10-4, 14/10-5, 14/10-9 and 14/15-4Z (Fig. 12). This may be a function of the core data representing sand-prone intervals within the wells. The injectites in other fans are more typically linked to the presence of hemi-limnic mudstones (i.e. in Sea Lion North and SL15; Fig. 13).

DISCUSSION

Sediment flow processes in injectites

The nature of the sedimentary flow processes operating within injectites are still a matter of debate. Dott (1966) and Taylor (1982) suggested that the flow processes are laminar, while Duranti (2007) and Hurst *et al*. (2011) suggest an early turbulent flow regime during the initial phases of hydrofracture propagation, followed by laminar flow during the later stages. The latter interpretation typically involves a complex combination of processes, leading to a variety of flow types and resultant deposits (Scott *et al*., 2009). Furthermore, intrusion events can stop abruptly when the fluid pressure in fractures drops below that of the local stress oriented parallel to the opening direction of the fracture, which can lead to grains freezing in place and injectites that lack sedimentary structure (Jonk, 2010). What is clear is that remobilized, fluidized sands can have complex transportation mechanisms, leading to a wide variety of sedimentary structures, or lack thereof, forming within clastic injectite systems.

The injectites of the SLIS contain a range of internal structures, the most enigmatic of these being ripple cross-lamination observed forming at sill margins (Figs 8 and 9B). The structures are interpreted to have formed through ripple migration within the sill, suggesting periods of dilute, probably sustained Newtonian fluid flow within the fracture network. A period of sustained fluid flow is also supported by the presence of imbricated mud-clasts (Fig. 8). The imbricated mud-clasts can also provide a proxy for flow direction in injectites (Kane, 2010; Ravier *et al*., 2015). In the examples provided in figure 8C, the ripple cross-lamination foresets dip towards the left, whereas the imbricated mud-clasts display opposing dips, towards the right. These two proxies suggest a consistent flow direction from right to left, but unfortunately in-situ flow directions could not be obtained as the core dataset is un-oriented. The sorting, deposition along ripple cross-lamination foresets, and imbrication suggests that the mud-clasts were fully-entrained into a relatively dilute fluid-sand mix; planar laminations developed at the upper sill contacts (Figs 8A and 8B) may support a flow that underwent sustained periods of traction (*sensu* Kawakami and Kawamura, 2002; Ravier *et al.*, 2015). Together, these observations support a period of sustained, relatively dilute, likely turbulent flow occurring within the fracture network of the SLIS.

The generation of ripple cross-lamination would be problematic if an injectite network is considered as a 'closed system' in which the injectites are not connected to the palaeo-sea floor. In this scenario, sediment concentrations are more likely to remain high (*sensu* Cobain, *et al.*, 2015), which might imply non-Newtonian fluid and therefore laminar flow behaviour, making ripple migration, under lower flow regime conditions, difficult to reconcile. However, if a clastic injectite network is considered as an 'open fracture' (T1 in Fig. 11), where fluids are free to move towards a palaeo-sea floor, sediment concentration can be diluted (*sensu* Cobain *et al*., 2015), flow can be sustained for longer periods of time, and a scenario for ripple migration is easier to perceive. An initial, period of sustained turbulent flow within the fracture network is the preferred scenario for the SLIS.

This initial period was followed by a subsequent 'closing fracture' phase (T2 in Fig. 11), as the fluid pressure in the injectite fell below stress perpendicular to the intrusion. During this time, the reduction of space within the fracture resulted in an increase in grain concentration, encouraging grain-on-grain interaction that acted to supress turbulence and resulted in more laminar flow conditions. Consequently, planar laminations in the centre of injectites (particularly in sills; Fig. 7A) are interpreted to have formed through the shearing of liquefied sand under laminar flow conditions during later periods of injection (Lowe, 1976; Allen, 1984; Hurst *et al*., 2011).

The interpretation of an early period of turbulent flow in the SLIS, followed by a later phase of laminar flow, confirms previous models of injectite development in other basins (Duranti, 2007; Scott *et al.,* 2009; Hurst *et al.,* 2011). This study therefore represents a case example of a spectrum of flow processes in operation during injectite emplacement, something that is still not fully understood (*cf.* Hurst *et al.,* 2011).

Style of emplacement

The style of emplacement for clastic injectites is ultimately controlled by the rheological properties of the host rocks and the driving forces acting on the sediment during deformation (Toro and Pratt, 2015). In the SLIS, host rocks typically comprise impermeable hemi-limnic mudstones, interbedded within thinly bedded sandstones forming a heterogeneous succession (Figs 13 and 14). This lithological heterogeneity can have a significant impact on the variety of deformation styles observed within the host rocks. This is shown best by a marked relationship between injectites and the light-grey to brown tuffs (tonsteins) within the mudstone intervals surrounding the Sea Lion Fan (Fig. 10). The injectites typically show a distinct change in emplacement style when they encounter these tuffs, which illustrates that the host rock properties influence, and are influenced by, the intrusion of the injectite systems.

The nature of injectite margins and the deformation of the host-strata can provide insights into the mechanical properties of the host material at the time of injection. In this study, injectite margins have been grouped into two end members: brittle margins, including stepped, smooth, and flat; and ductile margins, principally cuspate in form (distribution shown in Figure 13). Both groups can exhibit erosional characteristics at the margins, which form 'jagged' margins between the host rock and the sill (Figs 5C, 8D and 8E).

Brittle margin types form when fluidized sand intrudes into a relatively competent host rock (Cobain *et al.*, 2015). In the SLIS the presence of brittle margin types in both dykes (Figs 5A and 5D) and sills (Figs 7A, 7B, 7C, 8A and 8B) suggests that the host rocks were relatively competent during at least one period of intrusion. Furthermore, the observation of stepped margins (Figs 7A, 7B and 8A) is a good indicator for brittle deformation, which are widely documented, at a variety of different scales, within both clastic (Vétel and Cartwright, 2010; Cobain *et al.*, 2015) and igneous sills (Thomson and Hutton, 2004; Schofield *et al.*, 2012).

Other injectites in the SLIS, which display cuspate margins, particularly those that display lobate structures (Figs 5B, 5C, 6, 7D and 8C), are interpreted as emplacement through ductile deformation of relatively soft and probably uncompacted host material. Ptygmatic folding of the injectites (Figs 5A, 8C and 9C) attributable to post-depositional and post-injection compaction of both the host rock and the injectites, supports this style of emplacement (Kuenen, 1968; Hiscott, 1979; Parize *et al.*, 2007; Kane, 2010). Furthermore, a large proportion of the host rocks contain internal laminations that have been deformed by, or around, clastic dykes (Figs 5B, 6A, 6B, 9C and 10D). The deformation of laminations within the host rock may have occurred either during the intrusion event, or much later through differential compaction of mudstones around the more competent injectite structures (Fig. 14), both scenarios require relatively uncompacted host rocks to form. Finally, mud-clasts within injectites (Fig. 8) show a range of irregular, elongate and 'torn/rhomboid' geometries that together indicate they were relatively soft or ductile at the time of erosion and entrainment into the fluidized sand. These geometries are difficult to explain in a scenario where all of the mud-clasts were brittle or lithified during transport as they would otherwise be broken up within the flow.

There are clearly varying styles of deformation of host rocks formed during the emplacement of the SLIS. The observed geometries could be explained through a single phase of injection into host rock that displayed rheological anisotropy. The presence of brittle-ductile deformation structures and irregularities in injectite geometries has been previously linked to anisotropy within lithologically heterogeneous, mechanically variable strata (Truswell, 1972; Toro and Pratt, 2015; 2016). At shallow burial depths, compaction and lithification is likely to be anisotropic and controlled by lithological variability within a heterogeneous succession, which leads to a variety of mechanical properties. In this scenario, any intrusive event associated with injectite emplacement could deform the host sediments in a variety of styles, including in a ductile manner for the softer sediments, and a brittle manner for the harder, more-compact lithologies (Hurst *et al.*, 2011).

However, the preferred method of attaining the observed mixture of deformation styles in the SLIS is through multiple phases of emplacement, at shallow burial depths. In this scenario, there may have been an early injection phase whereby emplacement caused ductile deformation of uncompacted host rocks, potentially at shallower burial depths. The injectites, and in particular the dykes, were then ptygmatically folded during compaction and lithification. Subsequently, a second, or a series of injection events occurred in more consolidated sediments, resulting in brittle fracturing of lithified host rocks during emplacement. Evidence for multi-phased emplacement for the SLIS includes: variable injectite margin types (Fig. 13); mud-clasts that contain internal, sometimes ptygmatically folded injectites with cuspate margins (Figs 8A, 8C, 8E and 9B); and possibly the observed variability in visible cementation (i.e. Fig. 7) that may support emplacement by variable fluid types, at different burial depths and conditions (*sensu* Jonk *et al.*, 2005a); more work is required to address the latter hypothesis. Having multiple phases of injection that formed the SLIS is consistent with many other examples of injectite complexes, which typically record several injection episodes, at a range of burial depths (Duranti *et al.,* 2002; Hurst *et al.,* 2003a).

Intrusion mechanisms and depth of emplacement

Injectites are associated with a build-up of fluid overpressures, through a number of processes, and a subsequent trigger mechanism, which results in the re-mobilization of sand (Hurst *et al.*, 2011 and references therein). The build-up of overpressures is typically associated with fluid transfer (e.g. formation waters, hydrocarbons, etc.) within the subsurface, which is facilitated through a number of mechanisms, including disequilibrium compaction during burial (Osborne and Swarbrick, 1997), injection of fluids into a depositional sandstone, or load-induced over-pressuring (Hurst *et al*., 2011). Triggering mechanisms for injection are considered as either allogenic or autogenic.

Allogenic processes include impact or earthquake-related seismicity and are typically more unusual processes that lead to injectite formation (Hurst *et al.*, 2011 and references therein). Another, potentially more common allogenic triggering mechanism for injection is the rapid or accelerated migration of fluids into already over-pressured sandstones. These fluids can include: formation waters, e.g. bound waters released by the conversion of opal A into opal CT (Davies *et al.*, 2006; Ungerer *et al.*, 1981; Osborne and Swarbrick, 1997; Mann and Mackenzie, 1990); and oil and gas, which typically migrates at higher pressures from deeper within the basin (Lonergan *et al.*, 2000; 2002; Jonk *et al.*, 2005b). Given the proximity of the SLIS to the hydrocarbon-charged reservoirs of the Sea Lion, Casper and Beverley fans (Figs 3, 12 and 14), and considering the timing of oil generation of the North Falkland Basin petroleum system in general (as described in Richards and Hillier, 2000a; 2000b), the gradual and then accelerated migration of hydrocarbons from the deeply buried syn-rift source rocks up and into the shallow fan sandstones (Fig. 3) offers a plausible primer and triggering mechanism for the SLIS. The mechanism that permitted multiple phases of overpressure build up and triggering may have been related to pulsed hydrocarbon generation in deeper parts of the NFB, which lead to continued re-pressuring of the shallow system after the initial injection event.

In this scenario, hydrocarbon generation from source rocks located in the deeply-buried syn-rift stratigraphy in basin centre (as described in Richards and Hillier, 2000a; 2000b) possibly led to the build-up of palaeo-overpressures (priming mechanism) through the charging and migration of hydrocarbon fluids into the shallow, but sealed compartments of Sea Lion, Casper and Beverley fan sandstones (Figs 3 and 14). At some point, fluid migration may have accelerated, thereby providing a triggering mechanism necessary for injectite emplacement to occur. At present day, the Sea Lion, Casper and Beverley hydrocarbon reservoirs lack any evidence for over pressuring (figure 14 of MacAulay, 2015).

Finally, autogenic controls, such as instantaneous loading, must not be discounted, as they are often considered one of the most typical triggering mechanisms (Jonk, 2010; Hurst *et al.*, 2011). Injectites from the Vocontian Basin, Southern France, are interpreted as being formed within fractures during the emplacement of large volume, sandy flows (Parize and Fries, 2003). In the SLIS, high-volume sediment gravity flows (high density turbidites; Dodd *et al.,* 2019) and subsequent instantaneous loading of overlying fan deposits may have generated both primer and trigger conditions necessary for clastic intrusions to occur. It is possible that a proportion of the injectites observed within the SLIS are associated with relatively localised, autogenic processes, particularly those in close vertical proximity to depositional sandstone bodies.

One outcome from the analysis of injectites is to provide estimates for the depth of injectite emplacement within the subsurface. This is problematical and is often difficult to assess for many reasons (see Cobain *et al*., 2015), with only relative depth estimates being possible (i.e. shallow vs. deep). In the case of the SLIS, the presence of soft, uncompacted host rocks that display syn-injection ductile deformation of laminae and ptygmatic folding of dykes, suggests at least one period of intrusion occurred into uncompacted host-rocks, which could only have undergone limited burial at the time of injection. This suggests at least one phase of emplacement probably occurred relatively near to the palaeo-seafloor (Fig. 14). A second, or series of later phases of emplacement may have occurred slightly deeper (but still quite shallow), with emplacement occurring into more compacted, more brittle host rocks. This is supported by cuspate margins (and therefore shallow injection events) encountered throughout the SLIS, some of which occur over 60 m of compacted depth (Fig. 13), necessitating more than one shallow injection event. Finally, the apparent dominance of sill geometries over dykes, as observed in the SLIS (Fig. 12), has been used previously to suggest relatively shallow burial of host rocks at the time of injection (Hiscott, 1979; Jolly and Lonergan, 2002; Yang and Kim, 2014; Ravier *et al.*, 2015); although other workers (Vigorito *et al.,* 2008; Vetel and Cartwright, 2010) document sill-dominated intervals of injectite complexes occurring at much greater depths. Taking these observations into consideration, a general shallow emplacement depth for the SLIS is concluded in this study.

Spatial relationship between the injectites and the Sea Lion Fan

The distribution of the SLIS around the hydrocarbon-bearing Sea Lion, Beverley and Casper fans is important to consider as injectites can form fluid-flow conduits in the subsurface. Injectites are encountered throughout the LC3 sub-unit along the eastern flank of the North Falkland Basin, with a few observed within the uppermost deposits of the LC2 sub-unit (Figs 2 and 3). All but one cored well (14/10-5) contains evidence of injectites within mudstone prone successions (Fig. 13); no cored sections of wells were excluded from the dataset due to a lack of injectites. In general, the injectites tend to occur within the western and northern part of the Sea Lion Field (Fig. 1). Relatively dense occurrences are typically encountered directly above individual fans, particularly when there are overlying fan bodies present (injectites between SL10 and Casper; Figs 12, 13 and 14). The density of the injectites intersected in the core data suggest they are laterally pervasive features. This implies the fan bodies may be surrounded by halos of intruded hemi-limnic mudstones, which may have implications in terms of fluid flow between any isolated bodies of sandstone (over geological timescales).

The source of the remobilized sand (often termed the parent sand) is likely to be the adjacent, under and overlying turbidite fan deposits. This is based on their close spatial association between a depositional body and dense occurrences of injectites (Figs 1, 12 and 13), which is potentially documented in core data from well 14/15-4Z (Fig. 9A), although no re-fluidization features are observed in the underlying parent sandstone in that example. It is often difficult to accurately determine the exact origin of remobilized sand from core observations alone. Further studies, such as heavy-mineral assemblage analysis of sandstones intrusions and potential parent beds (*sensu* Hurst *et al.,* 2017*)*, would be required to better understand these relationships for the SLIS.

Impact on hydrocarbon exploration and reservoir modelling

In the SLIS, a large proportion of the injectites display visible porosity (62% of 143 injectites identified in this study; Figs 5B, 6A, 7A 6B, 8 and 15). Of those examples that display visible porosity 77% display oil staining (i.e. Fig. 7A). Measured core-plug porosity and permeability data from both sills and dykes (Fig. 15) display populations between *c.* 17–25% porosity, with permeabilities of *c.* 10–400 mD. In general, sills have higher porosities and permeabilities, although a population of dykes exists with *c.* 15–20% porosity and *c.* 10–70 mD permeability. When considered together, these observations suggest that, at some point in the past, the SLIS has formed an effective fluid network in the subsurface (Fig. 14).

It is also important to consider that a large proportion of the injectites in the SLIS are small, ranging between 0.8–70 cm in thickness for sills and from 0.25–11.2 cm in width for dykes (Fig. 15). In many scenarios, these features may be regarded as too small to form significant fluid conduits between otherwise disconnected reservoir bodies. However, given the relatively high density of the injectites intersected in the core data (143 injectites identified over 455 m of core), and considering the limited nature of subsurface core data (*c.* 12 cm wide core vs. 13 km wide fans), they are likely to be laterally and vertically pervasive away from the well locations. It is possible that, collectively, they could form effective fluid migration routes between any disconnected sandstone bodies (Fig. 14). Moreover, it is important to consider that small-scale features are often associated with much larger injection complexes (Ravier *et al*., 2015). It is quite possible that there will be slightly larger, sub-seismic-scale injectites (*c.* 1–12.5 m wide) in the direct vicinity of the Sea Lion, Casper and Beverley fans. In order to add to the general understanding of injectites, in particular the sub-seismic-scale features, quantitative data have been provided (Fig. 15), which could be included within reservoir models that need to incorporate the potential effects of sub-seismic-scale injectites on reservoir connectivity during production.

The global influence of injectites on fluid flow and hydrocarbon reservoir connectivity is generally well-known (Thompson, *et al.,* 1999; Lonergan *et al.,* 2000; Hurst *et al.,* 2003b). It is also well understood that an under appreciation for the presence and extent of clastic injectites can have both positive and negative consequences for modelling reservoirs for hydrocarbon production (Purvis *et al*., 2002). Therefore, an appreciation for potential heterogeneities provided by sub-seismic-scale injectites, in fine-scale reservoir models, is important in the accurate characterization of the subsurface around hydrocarbon reservoirs.

CONCLUSIONS

1. The 143 injectites of the SLIS contain a suite of sedimentary structures including: planar lamination, mud-clast sorting, mud-clast imbrication, ripple cross-lamination and structureless (sandstones).

2. Injectites are encountered in core data: above the Beaker 15 Fan and within/above the Sea Lion North Fan; within SL15 of the Sea Lion Fan; in-between SL10 of the Sea Lion Fan, and the Casper Fan; and above/below the Casper and Beverley fans.

3. The observation of mud-clast imbrication, along with ripple cross-lamination within sills suggests low concentration, Newtonian fluids potentially flowing in a turbulent manner within a hydraulically open fracture network. By contrast, the presence of planar laminations in injectite centres may be related to periods of laminar flow within a hydraulically-restricted fracture system.
4. In the SLIS, host rocks show evidence for ductile deformation and ptygmatic folding, suggesting they were relatively uncompacted during injection. However, stepped-margins indicate elements of brittle deformation during injection. This is attributed to multi-phased emplacement of injectites at different stages of host-rock lithification, at shallow burial depths.
5. The injectites of the SLIS display moderate porosity and permeability values, have visible oil staining, and therefore form potential fluid conduits. These examples highlight the potential of often overlooked, sub-seismic-scale injectites in forming effective fluid flow conduits in the subsurface, in general.

ACKNOWLEDGEMENTS

Phil Richards and Romesh Palamakumbura are thanked for their helpful review comments. Mario Vigorito and Sarah Cobain are thanked for their thorough and helpful reviews, which improved the manuscript. Adam McArthur and Ian Kane are thanked for editorial advice. The paper is published by permission of the Director, Mineral Resources, Falkland Islands Government, and the Executive Director, British Geological Survey (UKRI).

REFERENCES

Allen, J.R.L. (1984) Sedimentary Structures: Their Character and Physical Basis. *Elsevier, Amsterdam*.

Archer, J.B. (1984) Clastic intrusions in deep-sea fan deposits of the Rosroe Formation, Lower Ordovician, western Ireland. *Journal of Sedimentary Petrology*, **54**, 4 1197-1205.

Bunt, R.J.W. (2015) The use of seismic attributes for fan and reservoir definition in the Sea Lion Field, North Falkland Basin. *Petroleum Geoscience*, **21**, 137-149.

Cobain, S.L., Peakall, J. and **Hodgson, D.M.** (2015) Indicators of propagation direction and relative depth in clastic injectites: Implications for laminar versus turbulent flow processes. *Geological Society of America Bulletin*, **127**, 1816-1830.

Cobain, S.L. Hodgson, D.M., Peakall, J. and **Shiers, M.N.** (2017) An integrated model of clastic injectites and basin floor lobe complexes: implications for stratigraphic trap plays. *Basin Research*, **29**, 816-835.

Cosgrove, J.W. (2001) Hydraulic fracturing during the formation and deformation of a basin: A factor in the dewatering of low-permeability sediments: *American Association of Petroleum Geologists Bulletin*, **85**, 737–748.

Davies, R., Huuse, M., Hirst, P., Cartwright, J. and **Yang, Y.** (2006) Giant clastic intrusions primed by silica diagenesis. *Geological Society of America*, **34**, 917-920.

De Boer, W., Rawlinson, P.B. and Hurst, A. (2007) Successful Exploration of a Sand Injectite Complex: Hamsun Prospect, Norway Block 24/9. *In*: Hurst, A. and Cartwright, J. (eds) Sand injectites: Implications for hydrocarbon exploration and production: AAPG Memoir 87, 65–68.

Dixon, R.J., Schofield, K., Anderton, R., Renolds, A.D., Alexander, R.W.S., Williams, M.C. and **Davies, K.G.** (1995) Sandstone diapirism and clastic intrusion in the Tertiary submarine fans of the Bruce-Beryl Embayment, Quadrant 9, UKCS. *In*: Hartley, A.J. and Prosser, D.J. (eds) *Characterization of Deep Marine Clastic Systems: Geological Society of London Special Publication*, **94**, 77-94.

Dodd, T.J.H., McCarthy, D.J. and **Richards, P.C.** (2019) A depositional model for deep-lacustrine, partially confined, turbidite fans: Early Cretaceous, North Falkland Basin. *Sedimentology*, **66**, 53-80.

Dott, R.H. (1966). Cohesion and flow phenomena in clastic intrusions. *American Association of Petroleum Geologists Bulletin*, **50**, 610–611.

Duranti, D., Hurst, A., Bell, C., Groves, S. and **Hanson, R.** (2002) Injected and remobilised sands from the Alba Field (Eocene, UKCS): core and wireline log characteristics. *Petroleum Geoscience*, **8**, 99-107.

Duranti, D. and **Hurst, A.** (2004) Fluidization and injection in the deep-water sandstones of the Eocene Alba Formation (UK North Sea). *Sedimentology*, **51**, 503-529.

Duranti, D. (2007) Large-scale Sand Injection in the Palaeogene of the North Sea: Modeling of Energy and Flow Velocities. *In*: Hurst, A. and Cartwright, J. (eds) *Sand injectites: Implications for hydrocarbon exploration and production: AAPG Memoir*, **87**, 129-139.

Gamberi, F. (2010) Subsurface sediment remobilization as an indicator of regional-scale defluidization within the upper Tortonian Marnoso-arenacea formation (Apenninic foredeep, northern Italy). *Basin Research*, **22**, 562-577.

Gao, Y., Jiang, Z., Best, J.L., Liu, S. and Zhang, J. (2019) Small- and large- scale soft-sediment deformations in a Triassic lacustrine delta caused by overloading and seismicity in the Ordos Basin, central China. *Marine and Petroleum Geology*, **103**, 126-149.

Greensmith, J.T. (1957) A Sandstone Dyke near Queensferry, West Lothian. *Transactions of the Edinburgh Geological Society*, **17**, 54-59.

Google Earth 7.1. (2017) 6°06’12.46S, 81°53’08.372W to 67°21’20.632S, 0°26’24.892E. US Dept of State Geographer Image Landsat / Copernicus, Data SIO, NOAA, U.S. Navy, NGA, GEBCO. Viewed 18/07/2017

Goździk, J. and **Van Loom, A.J.** (2007) The origin of a giant downward directed clastic dyke in a kame (Bełchatów mine, central Poland). *Sedimentary Geology*, **193**, 71-79.

Hannum, C. (1980) Sandstone and Conglomerate-Breccia Pipes and Dikes of the Kodachrome Basin Area, Kane County, Utah. *Geological Studies Brigham Young University*, **27**, 31-50.

Hiscott, R.N. (1979) Clastic sills and dikes associated with deep-water sandstones, Tourelle Formation, Ordovician, Quebec. *Journal of Sedimentary Petrology*, **49**, 1, 0001-0010.

Hillier, R.D. and **Cosgrove, J.W.** (2002) Core and seismic observations of overpressure-related deformation within Eocene sediments of the Outer Moray Firth, UKCS. *Petroleum Geoscience*, **8**, 141-149.

Hubbard, S.M., Romans, B.W. and **Graham, S.A.** (2007) An outcrop example of large-scale conglomeratic intrusions sourced from deep-water channel deposits, Cerro Torro Formation, Magallanes basin, southern Chile. *In*: Hurst, A. and Cartwright, J. (eds) Sand Injectites: Implications for hydrocarbon exploration and production. *AAPG Memoir*, **87**, 199-207.

Hurst, A., Cartwright, J.A. and **Duranti, D.** (2003a) Fluidization structures produced by upward injection of sand through a sealing lithology. In: *Van Rensbergen, P., Hillis, R.R., Maltman, A.J., Morley, C.K. (Eds.), Subsurface Sediment Mobilization: Special Publication, Geological Society, London*, **216**, 123–137.

Hurst, A., Cartwright, J., Huuse, M., Jonk, R., Schwab, A., Duranti, D. and **Cronin, B.** (2003b) Significance of large-scale sand injectites as long-term fluid conduits: evidence from seismic data. *Geofluids*, **3**, 263-274.

Hurst, A., Cartwright, J.A., Duranti, D., Huuse, M. and **Nelson, M.** (2005) Sand injectites: an emerging global play in deep-water clastic environments. *In*: Doré, A.G. and Vining, B.A. (eds) *Petroleum Geology: North-West Europe and Global Perspectives – Proceedings of the 6th Petroleum Geology Conference*, 133-144. Geological Society, London.

Hurst, A. and **Cartwright, J.** (2007) Relevance of sand injectites to hydrocarbon exploration and production. *In*: Hurst, A., and Cartwright, J. (eds) *Sand injectites: Implications for hydrocarbon exploration and production*, AAPG Memoir **87**, 1-19

Hurst, A., Scott, A. and **Vigorito, M.** (2011) Physical characteristics of sand injectites. *Earth-Science Reviews*, **106**, 215-246.

Hurst, A., Huuse, M. Duranti, D. Vigorito, M. Jameson, E. and **Schwab, A.** (2016) Application of outcrop analogues in successful exploration of a sand injection complex, Volund Field, Norwegian North Sea. *Geological Society, London, Special Publications*, **436**, 75-92.

Hurst, A., Morton, A., Scott, A., Vigorito, M. and **Frei, D.** (2017) Heavy-mineral assemblages in sandstone intrusions: Panoche Giant Injection Complex, California, U.S.A., *Journal of Sedimentary Research*, **87**, 388-405.

Hurst, A. and **Vigorito, M.** (2017) Saucer-shaped sandstone intrusions: An underplayed reservoir target. *AAPG Bulletin*, **101**, 4, 625-633.

Huuse, M., Duranti, D, Steinsland, N., Guargena, C.G., Prat, P., Holm, K., Cartwright, J.A. and **Hurst, A.** (2004) Seismic Characteristics of Large-Scale Sandstone Intrusions in the Paleogene of the South Viking Graben, UK and Norwegian North Sea. *Geological Society of London, Memoirs*, **29**, 263-278.

Huuse, M., Cartwright, J., Hurst A., and **Steinsland N.** (2007) Seismic characterization of large scale sandstone intrusions. In A. Hurst and J. Cartwright (Eds) Sand injectites: Implications for hydrocarbon exploration and production: *AAPG Memoir*, **87**, 21-35.

Huuse, M., Jackson, C.A.L., Rensbergen, P.V., Davies, R.J., Fleming, P.B. and **Dixon, R.J.** (2010) Subsurface sediment remobilization and fluid flow in sedimentary basins: an overview. *Basin Research*, **22**, 342-360.

Jolly, R.J.H. and **Lonergran, L.** (2002) Mechanisms and controls on the formation of sand intrusions. *Journal of the Geological Society of London*, **159**, 605-617.

Jones, D.J.R., McCarthy, D.J. and **Dodd, T.J.H.** (2019) Tectonostratigraphy and the petroleum systems in the Northern sector of the North Falkland Basin, South Atlantic. *Marine and Petroleum Geology*, **103**, 150-162.

Jones, B.G. and **Rust, B.R.** (1983) Massive sandstone facies in the Hawkesbury Sandstones a Triassic fluvial deposit near Sydney, Australia. *Journal of Sedimentary Petrology*, **53**, 1249–1259.

Jonk, R., Duranti, D., Parnell, J., Hurst, A. and **Fallick, E.** (2003) The structural and diagenetic evolution of injected sandstones: examples from the Kimmeridgian of NE Scotland. *Journal of the Geological Society, London*, **160**, 881-894.

Jonk, R., Hurst, A., Duranti, D., Mazzini, A., Fallick, A.E. and **Parnell, J.** (2005a) The origin and timing of sand injection, petroleum migration and diagenesis: The Tertiary petroleum system of the south Viking Graben, North Sea. *American Association of Petroleum Geologists Bulletin* **89**, 329–357.

Jonk, R., Parnell and **Hurst, A.** (2005b) Aqueous and petroleum fluid flow associated with sand injectites. *Basin Research*, **17**, 241-257.

Jonk, R., Duranti, D., Hurst, A., Parnell, J. and **Fallick, A.E.** (2007) Aqueous and Petroleum Fluids Associated with Sand Injectites Hosted by Lacustrine Shales from the Oil-Shale Group (Dinantian), Midland Valley of Scotland. *In:* Hurst, A. and Cartwright, J. (eds) *Sand injectites: Implications for hydrocarbon exploration and production: AAPG Memoir* **87**, 265-274.

Jonk, R. (2010) Sand-rich injectites in the context of short-lived and long-lived fluid flow. *Basin Research*, **22**, 603-621.

Kane, I.A. (2010) Development and flow structures of sand injectites: The Hind Sandstone Member injectite complex, Carboniferous, UK. *Marine and Petroleum Geology*, **27**, 1200-1215.

Kawakami, G. and **Kawamura, M.** (2002) Sediment flow and deformation (SFD) layers: Evidence for intrastratal flow in laminated muddy sediments of the Triassic Osawa Formation, Northern Japan. *Journal of Sedimentary Research*, **72**, 1, 171-181.

Kuenen, Ph.H. (1968) Origin of ptygmatic features. *Tectonophysics*, **6**, 143-158.

Lohr, T. and **Underhill, J.R.** (2015) Role of rift transection and punctuated subsidence in the development of the North Falkland Basin. *Petroleum Geoscience*, **21**, 85-110.

Lorenz, J.C., Tuefel, L.W., and **Warpinski, N.R.** (1991) Regional Fractures I: A mechanism for the formation of regional fractures at depth in flat-lying reservoirs: *American Association of Petroleum Geologists Bulletin*, **75**, 1714–1737.

Lonergan, L., N. Lee, H. D. Johnson, J. A. Cartwright, and **R. J. H. Jolly,** (2000) Remobilization and injection in deepwater depositional systems: Implications for reservoir architecture and prediction. In: *P. Weimer, R. M. Slatt, J. Coleman, N. C. Rosen, H. Nelson, A. H. Bouma, M. J. Styzen, and D. T. Lawrence, eds., 13 deep-water reservoirs of the world: Gulf Coast Section SEPM Foundation 20th Annual Research Conference*, 515–532.

Lowe, D.R. (1975) Water escape structures in coarse-grained sediments. *Sedimentology*, **22**, 157-204.

Lowe, D.R. (1976). Subaqueous liquefied and fluidised sediment flows and their deposits. *Sedimentology* **23**, 285–308.

Lowe, D.R. (1979) Sediment gravity flows: their classification and some problems of application to natural flows and deposits. *SEPM Special Publication*, **27**, 75-82.

MacAulay, F. (2015) Sea Lion Field discovery and appraisal: a turning point for the North Falkland Basin. *Petroleum Geoscience*, **21**, 2-3.

Mann, D.M. and **Mackenzie, A.S.** (1990) Prediction of pore fluid pressures in sedimentary basins. *Marine and Petroleum Geology*, **7**, 55-65.

Monnier, D., Gay, A., Imbert, P., Cavailhes, T., Soliva, R. and **Lopex, M.** (2015) Sand injectites as a marker of the palaeo-stress field, the structural framework and the distance to the sand source: Example in the Vocontian Basin, SE France. *Journal of Structural Geology*, **79**, 1-18.

Murchison, R.I. (1827) Supplementary remarks on the oolitic series in the counties of Sutherland and Ross, and in the Hebrides. *Transactions of the Geological Society*, **2**, 353.

Mazzini, A., Duranti, D. Jonk, R., Parnell, J., Cronin, B.T., Hurst, A. and **Quine, M.** (2003) Paleo-carbonate seep structures above an oil reservoir, Gryphon Field, Tertiary, North Sea. *Geo-Mar Lett*, **23**, 323-339.

Newman, M.S.J., Reeder, M.L., Woodruff, A.H.W. and **Hatton, I.R.** (1993) The geology of the Gryphon Oil Field. In: Parker, J.R. (ed) *Petroleum Geology of Northwest Europe: Proceedings of the 4th Conference*, Geological Society of London, 123-133.

Osbourne, M.J. and **Swarbrick, R.E.** (1997) Mechanisms for generating overpressure in sedimentary basins: a re-evaluation. *AAPG Bulletin*, 81, 1023-1041.

Parize, O. and **Fries, G.** (2003) The Vocontian clastic dykes and sills: a geometric model. In: Van Rensbergen, P., Hillis, R.R., Maltman, A.J. and Morley, C.K. (eds) *Subsurface Sediment Mobilization. Geological Society, London, Special Publications,* **216**, 51-71.

Parize, O., Beaudoin, B., Champanhet, J., Friès, G., Imbert, P., Labourdette, R., Paternoster, B., Rubino, J. and **Schneider, F.** (2007) A Methodological Approach to Clastic Injectites From Field Analysis to Seismic Modeling – Examples of the Vocontian Aptian and Albian Injectites (Southeast France). In: *Hurst, A., Cartwright, J. (Eds.) Sand Injectites: Implications for Hydrocarbon Exploration and Production: American Association of Petroleum Geologists Memoir, Tulsa*, 173-190.

Peterson, G.L. (1968) Flow structures in sandstone dikes. *Sedimentary Geology*, **2**,3, 177-190.

Phillips, E., Everest, J. and **Reeves, H.** (2013) Micromorphological evidence for subglacial multiphase sedimentation and deformation during overpressurized fluid flow associated with hydrofracturing. *Boreas*, **42**, 395–427.

Pickering, K.T., Agar, S.M. and **Ogawa, Y.** (1988) Genesis and deformation of mud injections containing chaotic basalt-limestone-chert associations: Examples form the southwest Japan forearc. *Geology*, **16**, 881–885.

Pollard, D.D., Muller, O.H. and **Dockstader, D.R.** (1975) The Form and Growth of Fingered Sheet Intrusions. Geological Society of America Bulletin, **86**, 351-363.

Purvis, K., J. Kao, K. Flanagan, J. Henderson, and **D. Duranti**, (2002) Complex reservoir geometries in a deep water clastic sequence, Gryphon field, UKCS: Injection structures, geological modeling and reservoir simulation: *Marine and Petroleum Geology*, **19**, 161–179.

Ravier, E., Guiraud, M., Guillen, A., Vennin, E., Buoncristiani, J. and **Portier, E.** (2015) Micro- to macro-scale internal structures, diagenesis and petrophysical evolution of injectite networks in the Vocontian Basin (France): Implications for fluid flow. *Marine and Petroleum Geology*, **64**, 125-151.

Richards, P.C., Gatliff, R.W., Quinn, M.F. and **Fannin, N.G.T.** (1996a) Petroleum potential of the Falkland islands offshore area. *J. Petrol. Geol.*, **19**, 161–182.

Richards, P.C., Gatliff, R.W., Quinn, M.F., Williamson, J.P. and **Fannin, N.G.T.** (1996b) The geological evolution of the Falkland Islands continental shelf. In: *Weddel Sea Tectonics and Gondwana Break-up (Eds B.C. Storey, E.C. King and R.A. Livermore), Geol. Soc. Spec. Publ.*, **108**, 105–128.

Richards, P.C. and **Fannin, N.G.T.** (1997) Geology of the North Falkland Basin. *J. Petrol. Geol.*, **20**, 165–183.

Richards, P.C. and **Hillier, B.V.** (2000a) Post-drilling analysis of the North Falkland Basin – Part 1: Tectono-Stratigraphic Framework. *J. Petrol. Geol.*, **23**, 273-292.

Richards, P.C. and **Hillier, B.V.** (2000b) Post-drilling analysis of the North Falkland BASIN – Part 2: The petroleum system and future prospects. *Journal of Petroleum Geology*, **23**, 273–292.

Rowe, C.A., Mustard P.S., Mahoney, J.B. and **Katnick, D.C.** (2002) Oriented clastic dyke swarms as indicators of palaeoslope? An example from the Upper Cretaceous Nanaimo Group, Canada. *Journal of Sedimentary Research*, **72**, 1, 192-200.

Schofield, N.J., Brown, J.B., Magee, C. and **Stevenson, C.T.** (2012) Sill morphology and comparison of brittle and non-brittle emplacement mechanisms. *J. Geol. Soc.*, **169**, 127-141.

Scott, A., Vigorito, M., and **Hurst, A.** (2009) The process of sand injection: internal structures and relationships with host strata (Yellowbank Creek injectite complex, California, USA.). *Journal of Sedimentary Research*, **79**, 568-583.

Scott, A., Hurst, A. and **Vigorito, M.** (2013) Outcrop-based reservoir characterization of a kilometre-scale sand-injectite complex. *AAPG Bulletin*, **97**, 2, 309-343.

Smith, N.D. (1972) Flume experiments on the durability of mud clasts. *Journal of Sedimentary Petrology*, **42**, 378–383.

Smyers N.B. and **Peterson, G.L.** (1971) Sandstone Dikes and Sills in the Moreno Shale, Panoche Hills, California. *Geological Society of America Bulletin*, **82**, 3201-3208.

Svendsen, J.B., Hansen, H.J., Stærmose, T. and **Engkilde, K.** (2010) Sand remobilization and injection above an active salt diapir: the Tyr sand of the Nini Field, Eastern North Sea. *Basin Research*, **22**, 548-561.

Szarawarska, E., Huuse, M., Hurst, A., Boer, W.D., Lu, L., Molyneux, A. and **Rawlinson, P.** (2010) Three-dimensional seismic characterisation of large-scale sandstone intrusions in the lower Palaeogene of the North Sea: completely injected vs. *in situ* remobilised sandbodies. *Basin Research*, **22**, 517-532.

Taylor, B.J. (1982) Sedimentary dykes, pipes and related structures in the Mesozoic sediments of south-eastern Alexander Island. *British Antarctic Survey Bulletin,* **51**, 1–42.

Thompson, B.J., Garrison, R.E. and **Moore, C.J.** (1999) A late Cenozoic sandstone intrusion west of S. Cruz, California. Fluidized flow of water and hydrocarbon-saturated sediments. In: *Garrison, R.E., Aiello, I.W., Moore, J.C. (Eds.), Late Cenozoic Fluid Seeps and Tectonics along the San Gregorio Fault Zone in the Monterey Bay Region, California GB-76. Annual Meeting of the Pacific Section. American Association of Petroleum Geologists, Monterey, California,* 53–74.

Thompson, K. and **Hutton, D.** (2004) Geometry and growth of sill complexes: insights using 3D seismic from the North Rockall Trough. *Bulletin of Volcanology*, **66**, 364-375.

Töro, B. and **Pratt, B.R.** (2015) Characteristics and Implications of Sedimentary Deformation Features in the Green River Formation (Eocene) in Utah and Colorado. In: *Vanden Berg, M.D., Ressetar, R., and Birgenheier, L.P., editors, Geology of Utah's Uinta Basin and Uinta Mountains: Utah. Geological Association Publication*, **44**, 371-422.

Töro, B. and **Pratt, B.R.** (2016) Sedimentary record of seismic events in the Eocene Green River Formation and its implications for regional tectonics on lake evolution (Bridger Basin, Wyoming). *Journal of Sedimentary Geology*, **344**, 175-204.

Truswell, J.F. (1972) Sandstone sheets and related intrusions from Coffee Bay, Transkei, South Africa. *Journal of Sedimentary Petrology*, **42**, 578-583.

Ungerer, P., Behar, E. and **Discamps, D.** (1981) Tentative calculation of the overall volume expansion of organic matter during hydrocarbon genesis from geochemistry data. Implications for primary migration. *Advances in organic geochemistry*, **10**, 129-135.

Van der Meer, J.J.M., Kjær, K.H., Krüger, J., Rabassa, J. and **Kilfeather, A.A.** (2009) Under pressure: clastic dykes in glacial settings. *Quaternary Science Reviews*, **28**, 708–720.

Vigorito, M., Hurst, A., Cartwright, J. and **Scott, A.** (2008) Regional-scale subsurface sand remobilization: geometry and architecture. *Journal of the Geological Society, London*, **165**, 609-612.

Vigorito, M. and **Hurst, A.** (2010) Regional sand injectite architecture as a record of pore pressure evolution and sand redistribution in the shallow crust: insights from the Panoche Giant Injection Complex, California. *Journal of the Geological Society of London*, **167**, 889-904.

Vétel, W. and **Cartwright, J.** (2010) Emplacement mechanics of sandstone intrusions: insights from the Panoche Giant Injection Complex, California. *Basin Research*, **22**, 783-807.

Williams, L. (2015) Sedimentology of the Lower Cretaceous reservoirs of the Sea Lion Field, North Falkland Basin. *Petroleum Geoscience*, **21**, 183–198

Yang, S.Y. and **Kim, J.W.** (2014) Pliocene basin-floor fan sedimentation in the Bay of Bengal (offshore northwest Myanmar). *Marine and Petroleum Geology*, **49**, 45–58.

Figure Captions

Figure 1.) The location of the Falkland Islands with respect to South America (see inset map; modified after Google Earth, 7.1, 2017), along with the Mesozoic offshore basins, including the Malvinas, South Falkland, Falkland Plateau and the North Falkland basins. The Sea Lion North, Sea Lion, B15, Otter, Casper and Beverley fans were deposited along the eastern flank of the North Falkland Basin (see inset). Nine hydrocarbon exploration and appraisal wells intersect the fans. In six of these wells, 455 m of core data were collected, in which 143 injectites were encountered (injectite density marked by red circles).

Figure 2.) The tectono-stratigraphical framework of the early post-rift and middle post-rift sedimentary fill of the North Falkland Basin (after Richards and Hillier, 2000a). The Sea Lion North (SLN), Sea Lion (SL20, SL10 and SL15), Otter, Casper and Beverley fans were deposited in LC3, whilst the Bleaker Fan (B15) was deposited in LC2; both units occupying the early post-rift. The sand-rich fan deposits, along with the surrounding hemi-limnic mudstones, were intruded by the Sea Lion Injectite System.

Figure 3.) West-east oriented geoseismic section across the Eastern Graben and Eastern Flank of the NFB, near the Sea Lion Fan area (see figure 4 for section location). The 'transitional', 'early post-rift', 'middle post-rift' and 'late post-rift' tectono-stratigraphical sequences (as defined in Richards and Hillier, 2000a) represent significant rock units that contain the hydrocarbon system of the NFB. 'S' symbols in diamond polygons indicate the location of source rocks, whilst 'R' symbols in circular polygons indicate known reservoir intervals The Sea Lion Fan was deposited along the Eastern Flank. Whilst the stratigraphical positions of the 'B15', 'Casper' and 'Beverley' fans have been shown schematically (polygons with dotted outlines), they are not physically present in this section. The relative and stratigraphical distribution of injectites are marked and have been symbolised (not 'to-scale').

Figure 4.) 3D seismic character across the Sea Lion North, Sea Lion and Otter turbidite fans. Seismic data collected by Polarcus Limited. **A.)** Seismic amplitude extraction map from the Sea Lion North, Sea Lion and Otter fans (number of observed injectites in core data marked by white circles). **B.)** Cross-sectional view through a 3D seismic cube across the fans. The fans are tabular and often composed of a single seismic reflector. Intrusive geobodies are absent from within the seismic data, most likely as a consequence of the scale of the injectites and resolution limitations of the data set (*c.* <12.5 m not resolved). **C.)** A geoseismic interpretation of the fan geobodies and surrounding host mudstones.

Figure 5.) Examples of the wide variety of clastic dykes from the SLIS. **A.)** A ptygmatically folded, cemented dyke that displays smooth margins containing a number of 1–2 cm long mud-clasts (14/10-9Z, 2446.81–2447.00 m MDBRT). **B.)** A 3 cm wide dyke, displaying a cuspate margin with numerous lobate structures and aligned mud-clasts. A light-grey tuff has been deformed by, or around the intruding

sandstones (14/15-4Z, 2357.21–2357.33 m MDBRT). **C.)** An example of a clastic dyke with a jagged margin and 1–3 mm wide, aligned mud-clasts, forming a 'speckled texture' (14/15-4Z, 2449.23–2449.40 m MDBRT). A notable absence of mud-clasts occurs at, and below, the point where the jagged margin is observed, which could be related to a localised eddy in the flow formed as a consequence of interaction/erosion of the host rock wall. **D.)** An example of a clastic dyke, which displays smooth margins and is filled with 1–4 cm long, elongate, aligned mud-clasts. The alignment of mud-clasts is commonly observed within the SLIS, particularly within the thinner examples of dykes (14/10-3, 2496.30–2496.43 m MDBRT).

Figure 6.) Examples of dyke to sill transitions from the SLIS. **A.)** A 20 cm long, 5 cm wide dyke cutting up stratigraphy and feeding into a sill at the top. The host rocks comprise laminated sandstones and siltstones, along with chaotic-textured depositional units. The depositional sediments display ductile deformation, indicating they were deformed by, or around, the clastic dyke. The injected sandstones display visible porosity, along with oil staining (14/10-3, 2489.37–2489.58m MDBRT). **B.)** A 45° clastic dyke feeding into a horizontal sill with reverse displacements observed within the host rocks, representing a small-scale 'jack-up' structure. Both the clastic dyke and sill display visible porosity, along with oil staining (14/10-3, 2468.10–2468.25 m MDBRT).

Figure 7.) A variety of sills and sill-margin types from the SLIS. **A.)** An example of an oil-stained sill, displaying a stepped margin and planar laminations (14/15-4Z, 2453.13–2453.27 m MDBRT). **B.)** An example of a cemented structureless sill, with a stepped upper margin (14/15-4Z, 2445.85–2445.96 m MDBRT). **C.)** An example of a 0.5 cm thick sill, documenting stepped margins at a smaller scale (14/15-4Z, 2449.12–2449.18 m MDBRT). **D.)** A porous sill with erosional margins, where in-situ mud-clasts are preserved in the process of being eroded from the host rock (14/10-9Z, 2455.04–2455.08 m MDBRT).

Figure 8.) Images of core data (left) and interpreted sections of core (right). **A.)** An example of a 12 cm thick sill, displaying a stepped margin, along with well-developed clast alignment and imbrication near to the lower margin. A large proportion of the imbricated mud-clasts display a common dip towards the right of the photo, with some localised mud-clasts that dip in the opposite direction (14/15-4Z, 2474.42–2474.61 m MDBRT). **B.)** An example of a 12 cm thick sill, with well-developed clast-alignment and imbricated mud-clasts that dip to the right of the photo (14/15-4Z, 2475.76-2475.87 m MDBRT). **C.)** A zoomed-in view of the foresets shown in figure 8A. Five different foresets are shown (labelled 1–5), which display variations in mud-clast concentrations and sizes. The large mud-clast at the top has stepped margins and internally contains an injectite with cuspate margins, which is ptygmatically folded. **D.)** An example of a *c.* 10 cm thick sill (14/10-3, 2499.15 m MDBRT), which is fed by (or feeds into) a series of smaller injectites present both above and below the feature. The white box denotes the area shown as a 'close-up' in figure 8E. **E.)** A 'close-up' view of the basal section of the sill from figure

8D, showing examples of mud-clasts that are: internally injected and irregular in shape; torn or rhomboid; imbricated, dipping to the right of the photo; and are sorted into varying sizes and concentrations. Like with other examples, 'foresets' are visible at the base of the sill (labelled 1–5).

Figure 9.) A 35 cm thick sill, overlying a depositional sandstone unit, encountered in-between the Casper Fan and the overlying Beverley Fan (see Fig. 12; 14/15-4Z, 2428.60–2431.81 m MDBRT). **A.)** The sill displays sharp upper and lower contacts and is composed of well-sorted, fine to medium-grained sandstones that display visible porosity, oil-staining and averaged porosity/permeability values 13.8% and 33.4 mD, respectively. The underlying depositional sandstone interval may represent the parent unit for the overlying injectite system. **B.)** The well-sorted sandstone matrix of the sill shown in figure 9A, which contains a number of mud-clasts, along with poorly-developed ripple cross-lamination at the top. A *c.* 8 cm wide clast, encountered towards the top of the sill displays angular edges and internal injectites that display lobate margins and ptygmatic folding. The position of figure Bi is marked by the white box. **Bi.)** A 'close-up' of the mud-clast boundary documenting a difference in grain size between the sandstone matrix of the sill (fine-grained) compared with the sandstone matrix of the internal injectite within the mud-clast (very fine-grained). **C.)** An example of intruded host rock from directly above the parent sandstone (see figure 9A for the location of this image), documenting a ptygmatically folded dyke (note – some drilling-related core breakage in this section).

Figure 10.) Examples of injectites intruding into light-grey to medium-brown tuffs (tonsteins). There is a clear spatial relationship between the presence of injectites and the tuffs within the core, with the injectites often exploiting these mechanically weaker intervals. **A.)** A near vertical dyke that interacts with a tuff resulting in the 'thinning-out' of siliceous material, along with micro-fracturing (14/10-9Z, 2444.79–2444.85 m MDBRT). **B.)** An example of a clastic dyke cutting into the edge of a tuff (14/10-9Z, 2444.80–2444.85 m MDBRT). **C.)** A clastic sill intruding completely within a tuff representing a zone of weakness (14/10-9Z, 2451.60–2451.82 m MDBRT). **D.)** A clastic dyke arcing down and through a tuff, illustrating the preferential relationship between dyke emplacement and the zones of weakness (14/10-9Z, 2453.66–2453.79 m MDBRT).

Figure 11.) A conceptual model for the infilling of clastic sills with sediment. **A.)** At 'T1', the ripple cross-lamination is developed during a period when the fracture is open and the sill-dyke systems are connected to the palaeo-seafloor. The migration of the ripple bedforms can only take place if the fluid concentrations were sufficiently dilute, which might imply an open fracture. Note the erosion of mud-clasts from the host rock that contain internal injectites. **B.)** At 'T2', the fracture is beginning to close or is about to close, with the compression resulting in an increase in sediment concentrations and the development of laminar flow. Eventually, this results in the in-situ freezing of typically structureless or planar laminated, well-sorted sand, which effectively infills the remaining space in the fracture.

Commonly, this late-stage flow infills the centre of a sill, but theoretically could be found anywhere within the fracture.

Figure 12.) A broadly north-south oriented (see inset) wireline correlation of cored wells. The vertical position in the well and injectite type (sill or dyke shown in red or blue, respectively) are illustrated. The injectites are distributed in four groupings: above the Bleaker 15 Fan (B15) and within/above the Sea Lion North Fan (SLN); within the Sea Lion 15 lobe (SL15) of the Sea Lion Fan; overlying the Sea Lion Fan, chiefly above the Sea Lion 10 lobe (SL10); and above/below the Casper and Beverley Fans.

Figure 13.) Sedimentary logs of cored intervals within wells that intersect the Sea Lion North (SLN), Bleaker 15 (B15), Sea Lion (SL; 20, 15 and 20), Casper (CA), and Beverley (BEV) fans. The sedimentary logs are coloured in terms of facies associations, using the facies model set out in Dodd *et al.,* 2019. The position of the 143 injectites has been plotted, with dyke or sill geometries recorded as a blue and red bar, respectively. Margin types, including: smooth; cuspate; stepped; flat; erosional; and jagged, have been plotted to demonstrate vertical (and in some respects lateral) distribution of injectite morphology.

Figure 14.) A conceptual 3D block diagram (schematic), illustrating the distribution, style and geometries of injectites observed in the core data through the SLIS, and their relationship with the Bleaker 15 (B15), Sea Lion North (SLN), Sea Lion (SL20, SL15 and SL10), Casper, and Beverley fans. The injectites of the SLIS have the potential to form fluid conduits between any disconnected reservoir intervals, and may have facilitated more effective hydrocarbon migration and charge through the succession.

Figure 15.) Quantitative data from the 143 injectites of the SLIS, which could be used to populate fine-scale reservoir models that need to incorporate the potential effects of sub-seismic-scale injectites. **A.)** Scatter plot of core-plug porosity vs. permeability (logarithmic) from both dykes and sills. A linear trend of increasing permeability with increasing porosity is displayed. In general, sills display higher porosities and permeabilities than dykes. **B.)** Sill thicknesses (cm) within the SLIS. **C.)** Visible porosity in the injectites, observable in core data. **D.)** Dyke heights (cm) in core data, with most reaching up to 25 cm. **E.)** Dyke width (cm) observed in core data. The upper limit of dyke width is limited by the diameter of the core data (*c.* 12 cm).

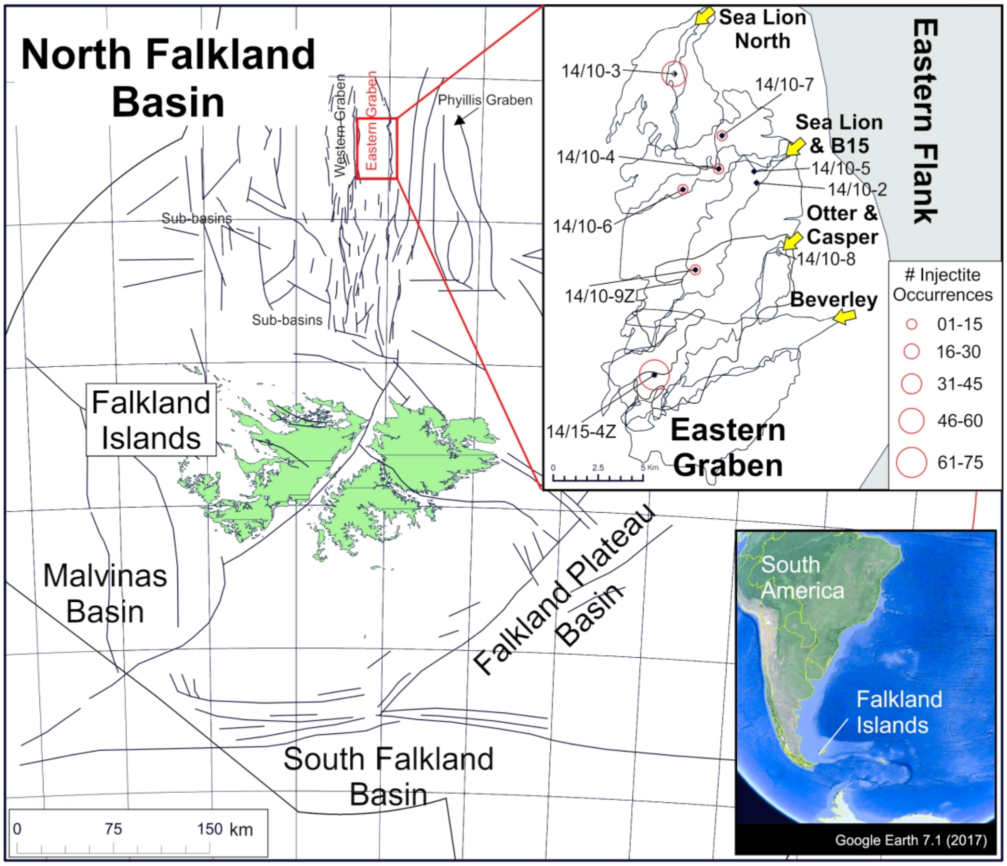

Figure 1

Figure 1.) The location of the Falkland Islands with respect to South America (see inset map; modified after Google Earth, 7.1, 2017), along with the Mesozoic offshore basins, including the Malvinas, South Falkland, Falkland Plateau and the North Falkland basins. The Sea Lion North, Sea Lion, B15, Otter, Casper and Beverley fans were deposited along the eastern flank of the North Falkland Basin (see inset). Nine hydrocarbon exploration and appraisal wells intersect the fans. In six of these wells, 455 m of core data were collected, in which 143 injectites were encountered (injectite density marked by red circles).

200x178mm (300 x 300 DPI)

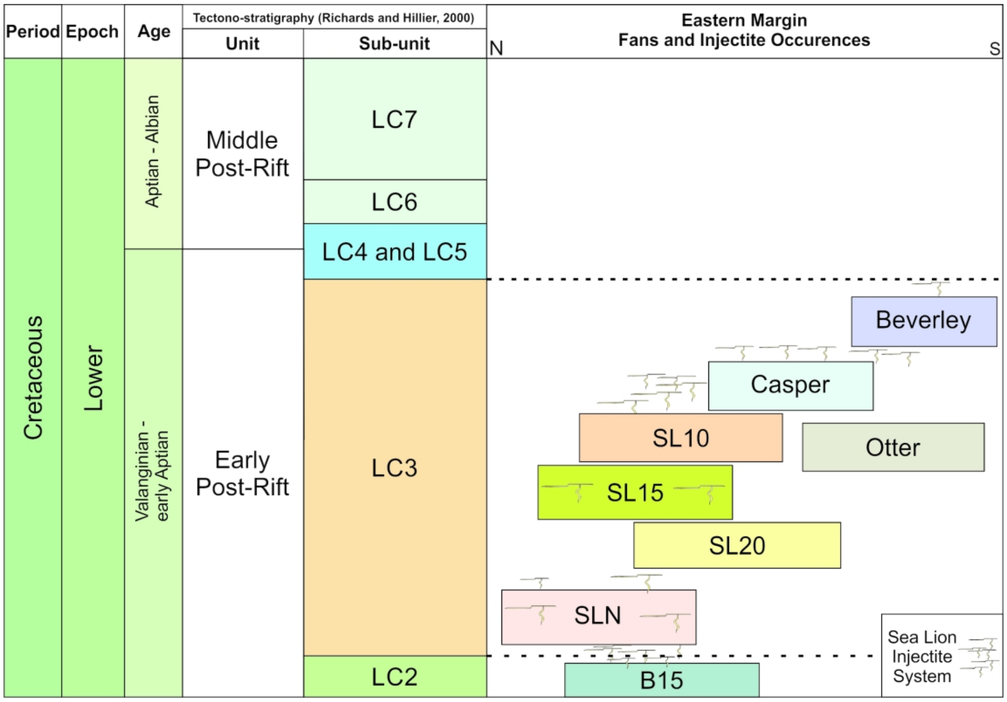

Figure 2

Figure 2.) The tectono-stratigraphical framework of the early post-rift and middle post-rift sedimentary fill of the North Falkland Basin (after Richards and Hillier, 2000a). The Sea Lion North (SLN), Sea Lion (SL20, SL10 and SL15), Otter, Casper and Beverley fans were deposited in LC3, whilst the Bleaker Fan (B15) was deposited in LC2; both units occupying the early post-rift. The sand-rich fan deposits, along with the surrounding hemi-limnic mudstones, were intruded by the Sea Lion Injectite System.

202x145mm (300 x 300 DPI)

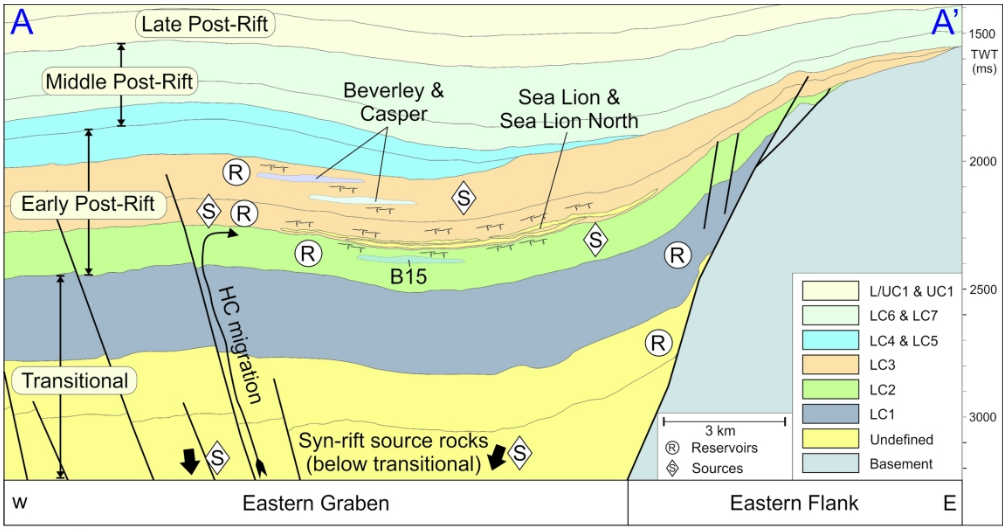

Figure 3

Figure 3.) West-east oriented geoseismic section across the Eastern Graben and Eastern Flank of the NFB, near the Sea Lion Fan area (see figure 4 for section location). The 'transitional', 'early post-rift', 'middle post-rift' and 'late post-rift' tectono-stratigraphical sequences (as defined in Richards and Hillier, 2000a) represent significant rock units that contain the hydrocarbon system of the NFB. 'S' symbols in diamond polygons indicate the location of source rocks, whilst 'R' symbols in circular polygons indicate known reservoir intervals The Sea Lion Fan was deposited along the Eastern Flank. Whilst the stratigraphical positions of the 'B15', 'Casper' and 'Beverley' fans have been shown schematically (polygons with dotted outlines), they are not physically present in this section. The relative and stratigraphical distribution of injectites are marked and have been symbolised (not 'to-scale').

202x111mm (300 x 300 DPI)

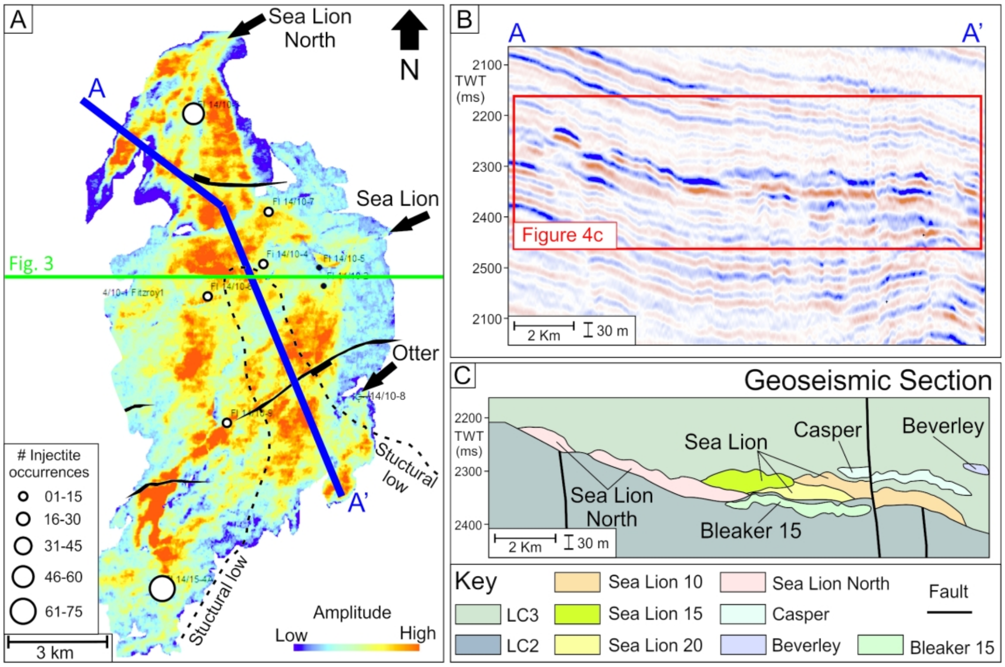

Figure 4

Figure 4.) 3D seismic character across the Sea Lion North, Sea Lion and Otter turbidite fans. Seismic data collected by Polarcus Limited. A.) Seismic amplitude extraction map from the Sea Lion North, Sea Lion and Otter fans (number of observed injectites in core data marked by white circles). B.) Cross-sectional view through a 3D seismic cube across the fans. The fans are tabular and often composed of a single seismic reflector. Intrusive geobodies are absent from within the seismic data, most likely as a consequence of the scale of the injectites and resolution limitations of the data set (c. <12.5 m not resolved). C.) A geoseismic interpretation of the fan geobodies and surrounding host mudstones.

200x138mm (300 x 300 DPI)

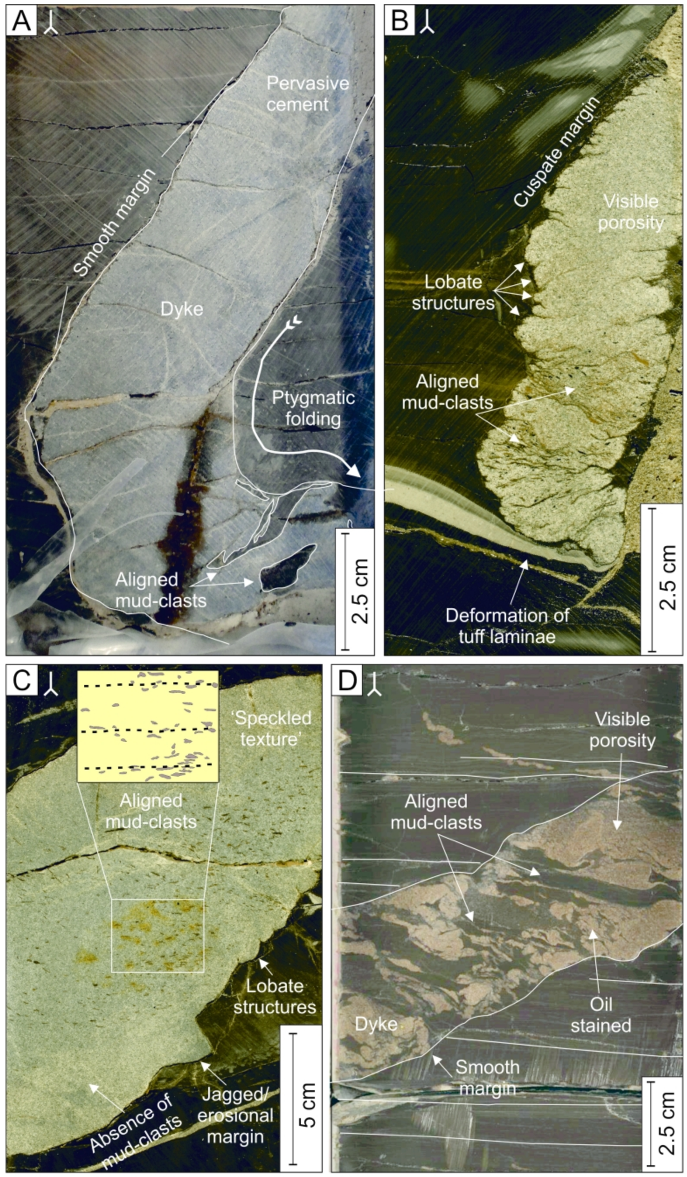

Figure 5

Figure 5.) Examples of the wide variety of clastic dykes from the SLIS. A.) A ptygmatically folded, cemented dyke that displays smooth margins containing a number of 1–2 cm long mud-clasts (14/10-9Z, 2446.81–2447.00 m MDBRT). B.) A 3 cm wide dyke, displaying a cuspate margin with numerous lobate structures and aligned mud-clasts. A light-grey tuff has been deformed by, or around the intruding sandstones (14/15-4Z, 2357.21–2357.33 m MDBRT). C.) An example of a clastic dyke with a jagged margin and 1–3 mm wide, aligned mud-clasts, forming a 'speckled texture' (14/15-4Z, 2449.23–2449.40 m MDBRT). A notable absence of mud-clasts occurs at, and below, the point where the jagged margin is observed, which could be related to a localised eddy in the flow formed as a consequence of interaction/erosion of the host rock wall. D.) An example of a clastic dyke, which displays smooth margins and is filled with 1–4 cm long, elongate, aligned mud-clasts. The alignment of mud-clasts is commonly observed within the SLIS, particularly within the thinner examples of dykes (14/10-3, 2496.30–2496.43 m MDBRT).

151x268mm (300 x 300 DPI)

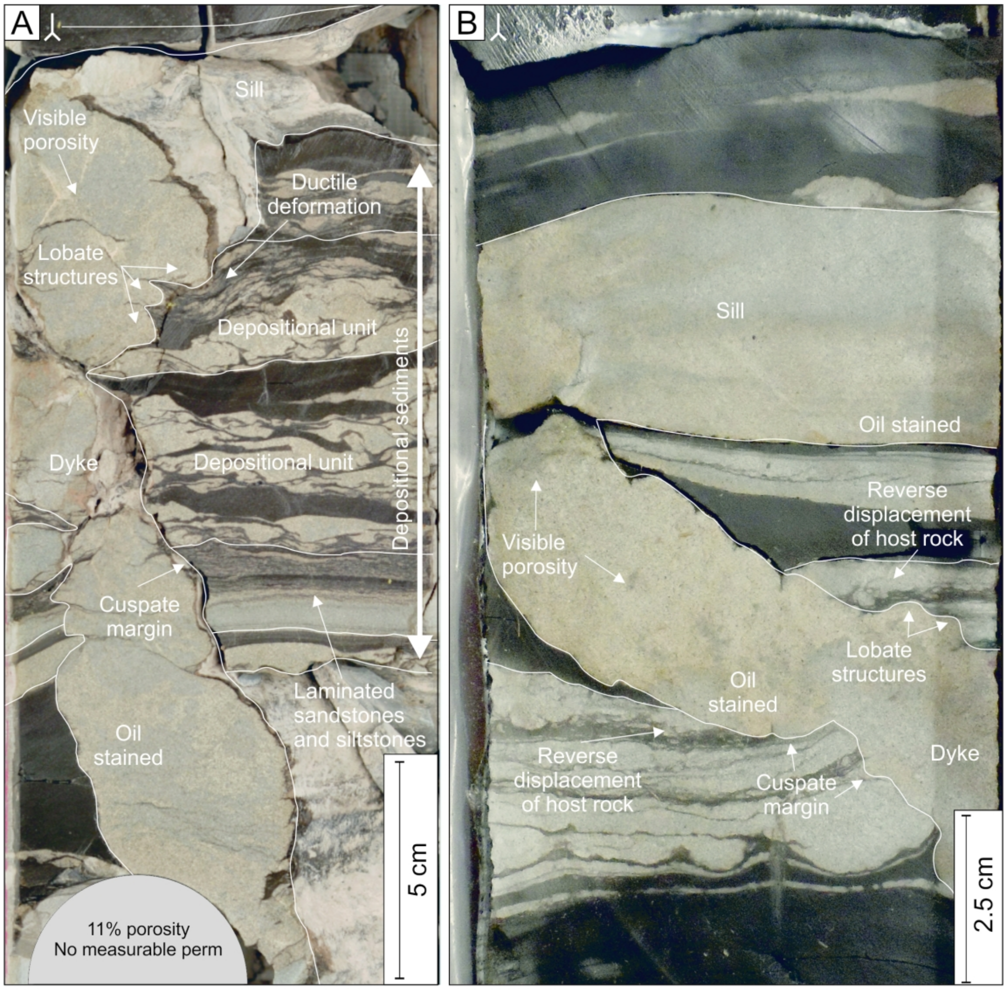

Figure 6

Figure 6.) Examples of dyke to sill transitions from the SLIS. A.) A 20 cm long, 5 cm wide dyke cutting up stratigraphy and feeding into a sill at the top. The host rocks comprise laminated sandstones and siltstones, along with chaotic-textured depositional units. The depositional sediments display ductile deformation, indicating they were deformed by, or around, the clastic dyke. The injected sandstones display visible porosity, along with oil staining (14/10-3, 2489.37–2489.58m MDBRT). B.) A 45° clastic dyke feeding into a horizontal sill with reverse displacements observed within the host rocks, representing a small-scale 'jack-up' structure. Both the clastic dyke and sill display visible porosity, along with oil staining (14/10-3, 2468.10–2468.25 m MDBRT).

196x197mm (300 x 300 DPI)

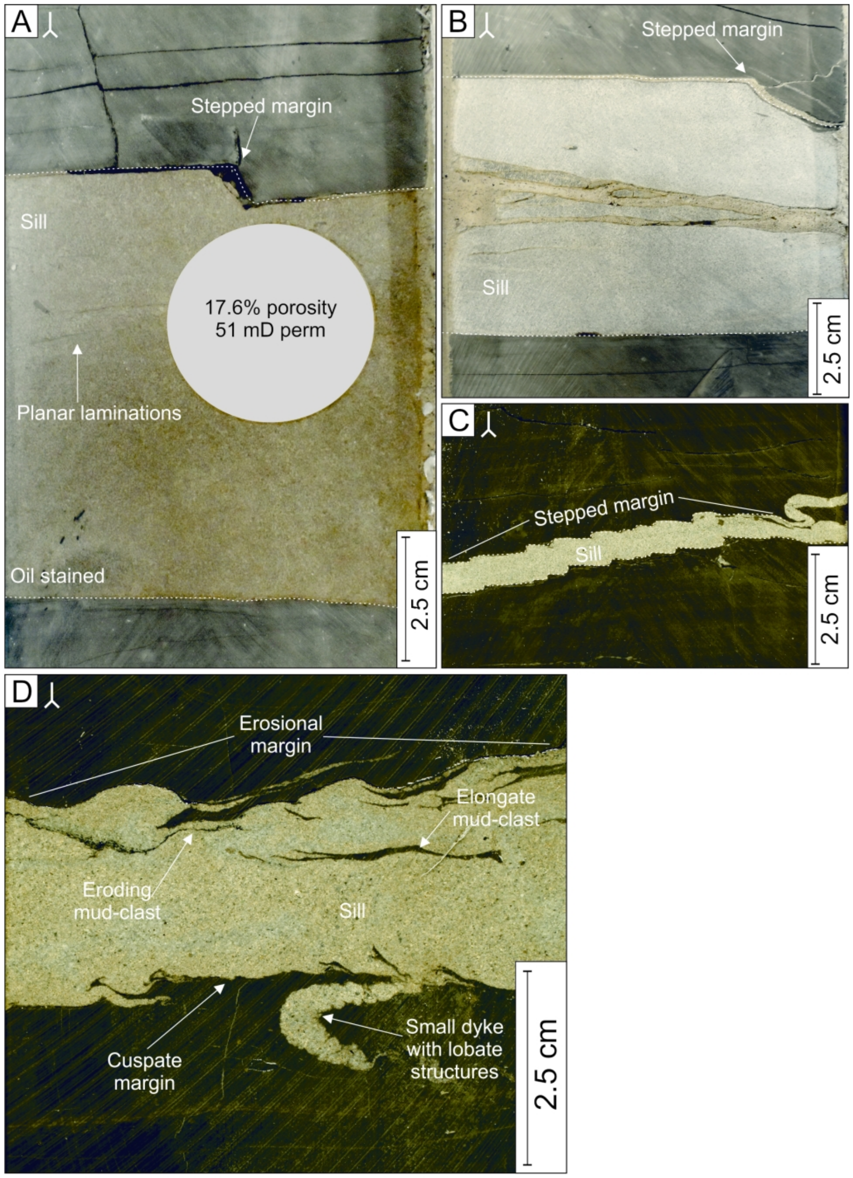

Figure 7

Figure 7.) A variety of sills and sill-margin types from the SLIS. A.) An example of an oil-stained sill, displaying a stepped margin and planar laminations (14/15-4Z, 2453.13–2453.27 m MDBRT). B.) An example of a cemented structureless sill, with a stepped upper margin (14/15-4Z, 2445.85–2445.96 m MDBRT). C.) An example of a 0.5 cm thick sill, documenting stepped margins at a smaller scale (14/15-4Z, 2449.12–2449.18 m MDBRT). D.) A porous sill with erosional margins, where in-situ mud-clasts are preserved in the process of being eroded from the host rock (14/10-9Z, 2455.04–2455.08 m MDBRT).

181x253mm (300 x 300 DPI)

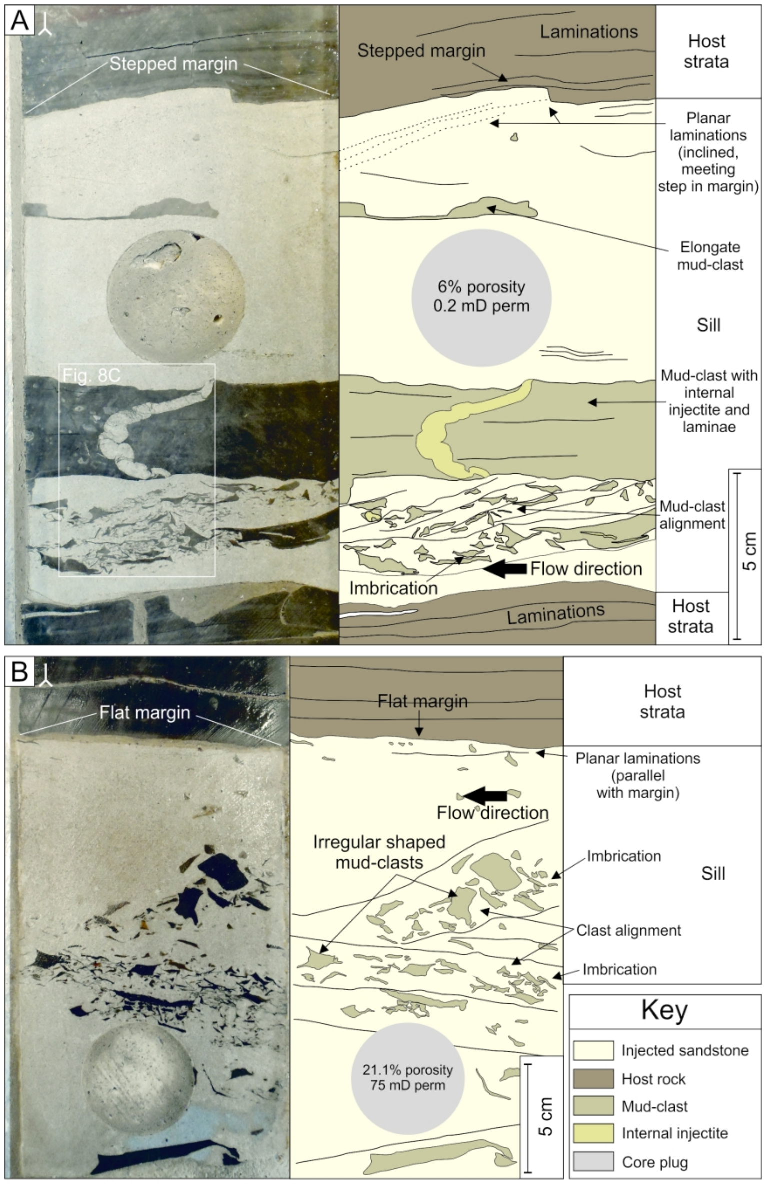

Figure 8A and 8B

Figure 8.) Images of core data (left) and interpreted sections of core (right). A.) An example of a 12 cm thick sill, displaying a stepped margin, along with well-developed clast alignment and imbrication near to the lower margin. A large proportion of the imbricated mud-clasts display a common dip towards the right of the photo, with some localised mud-clasts that dip in the opposite direction (14/15-4Z, 2474.42–2474.61 m MDBRT). B.) An example of a 12 cm thick sill, with well-developed clast-alignment and imbricated mud-clasts that dip to the right of the photo (14/15-4Z, 2475.76-2475.87 m MDBRT).

176x278mm (300 x 300 DPI)

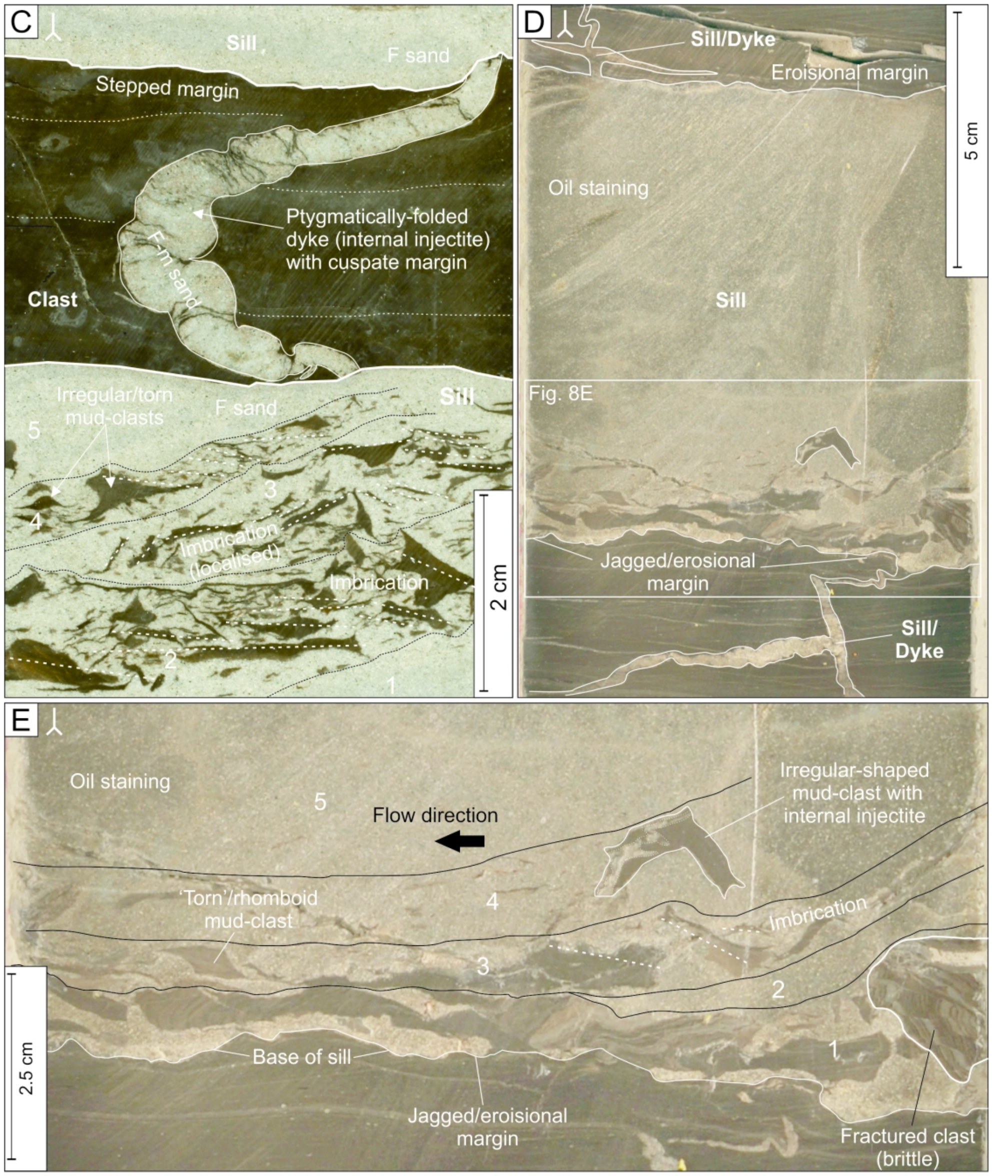

Figure 8C, 8D and 8E

Figure 8. (cntd) C.) A zoomed-in view of the foresets shown in figure 8A. Five different foresets are shown (labelled 1–5), which display variations in mud-clast concentrations and sizes. The large mud-clast at the top has stepped margins and internally contains an injectite with cuspate margins, which is ptygmatically folded. D.) An example of a c. 10 cm thick sill (14/10-3, 2499.15 m MDBRT), which is fed by (or feeds into) a series of smaller injectites present both above and below the feature. The white box denotes the area shown as a 'close-up' in figure 8E. E.) A 'close-up' view of the basal section of the sill from figure 8D, showing examples of mud-clasts that are: internally injected and irregular in shape; torn or rhomboid; imbricated, dipping to the right of the photo; and are sorted into varying sizes and concentrations. Like with other examples, 'foresets' are visible at the base of the sill (labelled 1–5).

204x249mm (300 x 300 DPI)

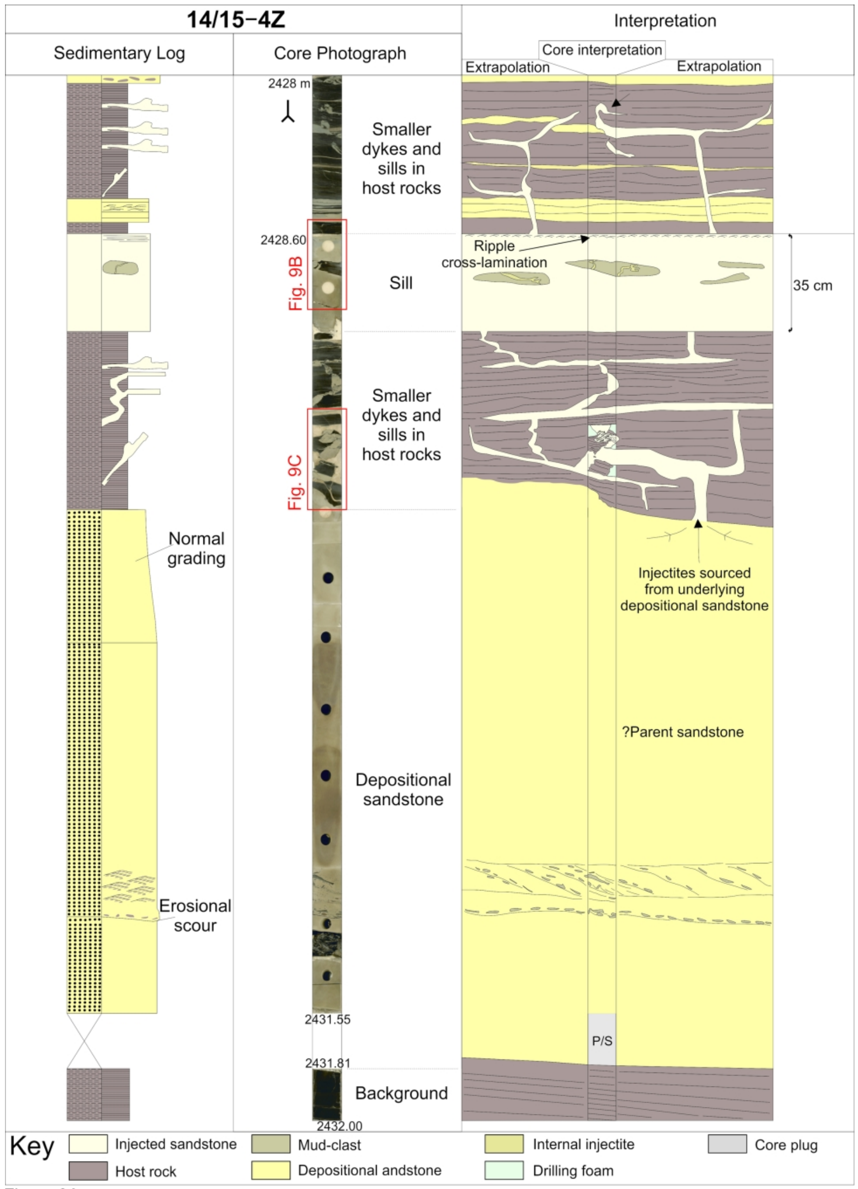

Figure 9A

Figure 9.) A 35 cm thick sill, overlying a depositional sandstone unit, encountered in-between the Casper Fan and the overlying Beverley Fan (see Fig. 12; 14/15-4Z, 2428.60–2431.81 m MDBRT). A.) The sill displays sharp upper and lower contacts and is composed of well-sorted, fine to medium-grained sandstones that display visible porosity, oil-staining and averaged porosity/permeability values 13.8% and 33.4 mD, respectively. The underlying depositional sandstone interval may represent the parent unit for the overlying injectite system.

206x291mm (300 x 300 DPI)

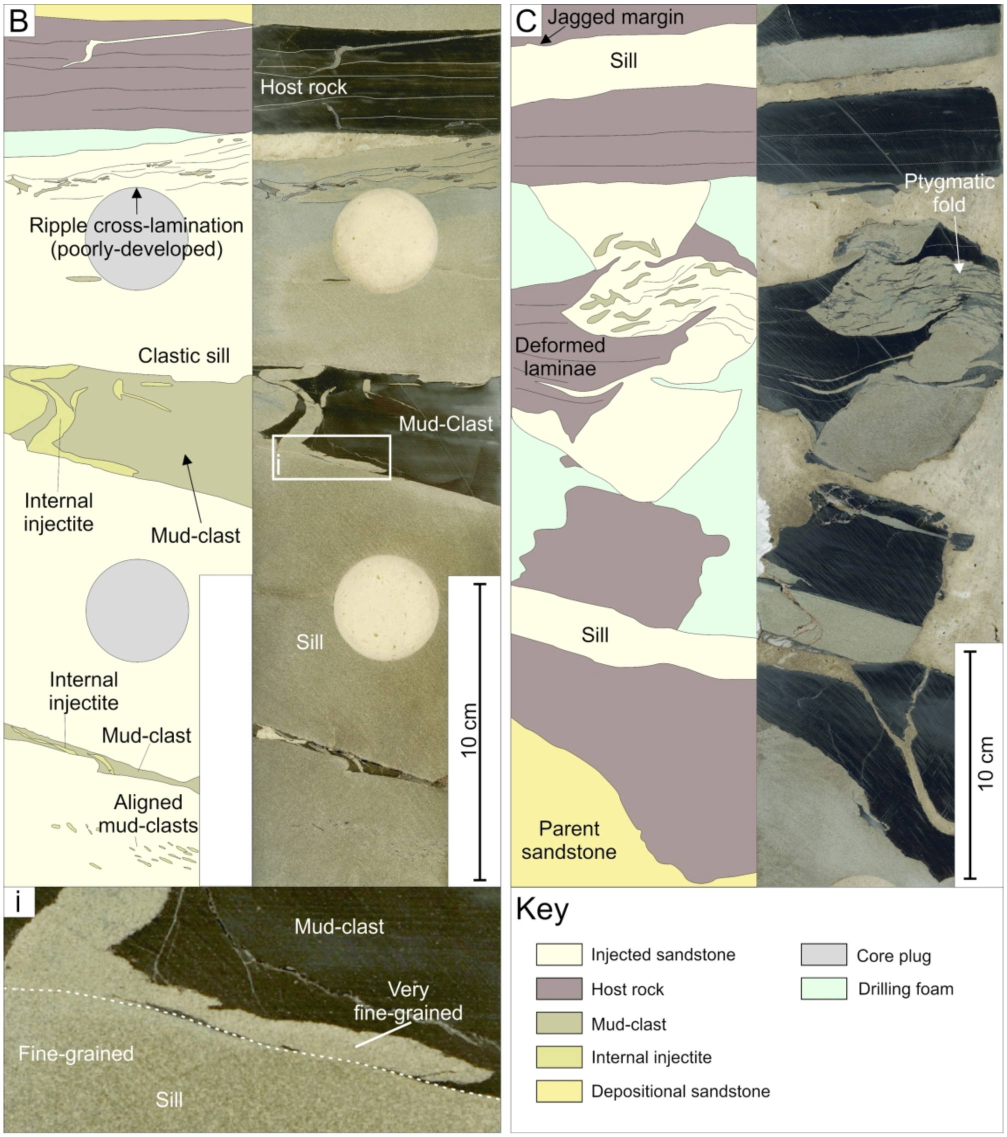

Figure 9B and 9C

Figure 9. (cntd) B.) The well-sorted sandstone matrix of the sill shown in figure 9A, which contains a number of mud-clasts, along with poorly-developed ripple cross-lamination at the top. A c. 8 cm wide clast, encountered towards the top of the sill displays angular edges and internal injectites that display lobate margins and ptygmatic folding. The position of figure Bi is marked by the white box. Bi.) A 'close-up' of the mud-clast boundary documenting a difference in grain size between the sandstone matrix of the sill (fine-grained) compared with the sandstone matrix of the internal injectite within the mud-clast (very fine-grained). C.) An example of intruded host rock from directly above the parent sandstone (see figure 9A for the location of this image), documenting a ptygmatically folded dyke (note – some drilling-related core breakage in this section).

204x237mm (300 x 300 DPI)

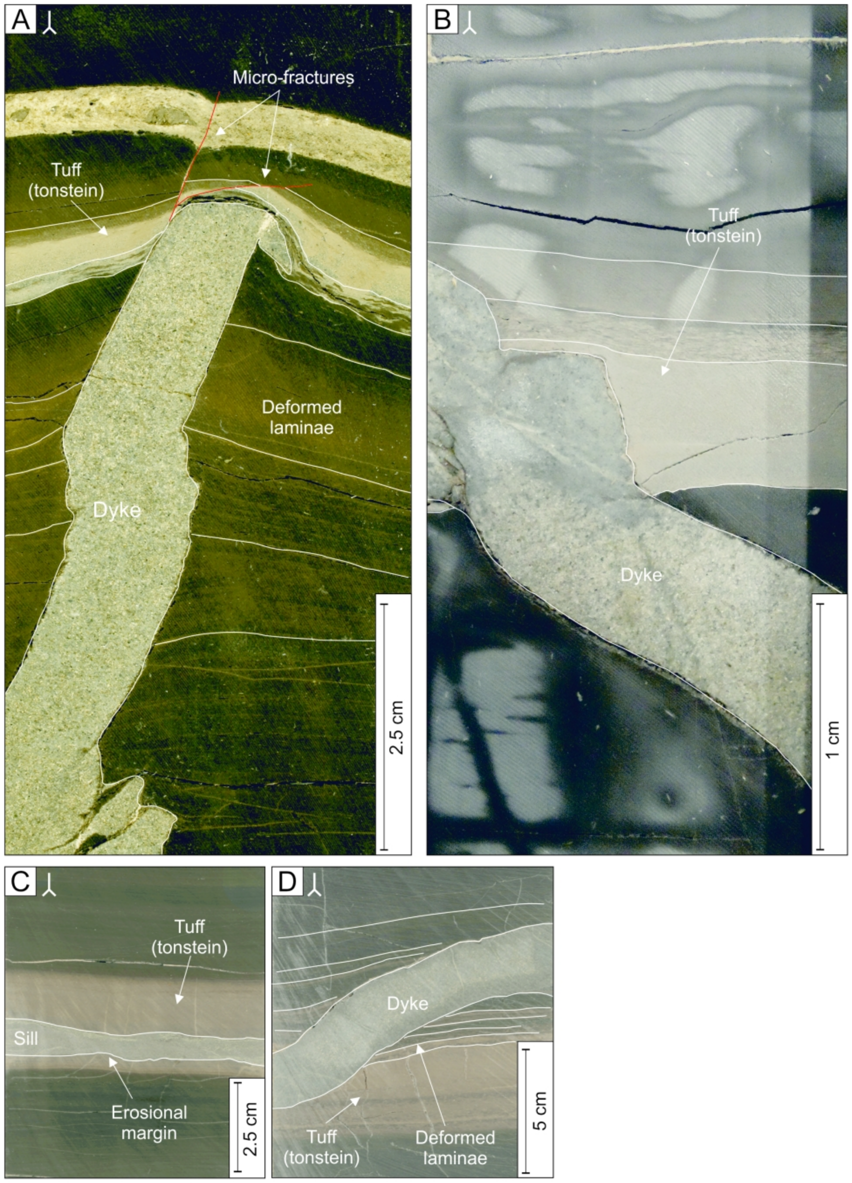

Figure 10

Figure 10.) Examples of injectites intruding into light-grey to medium-brown tuffs (tonsteins). There is a clear spatial relationship between the presence of injectites and the tuffs within the core, with the injectites often exploiting these mechanically weaker intervals. A.) A near vertical dyke that interacts with a tuff resulting in the 'thinning-out' of siliceous material, along with micro-fracturing (14/10-9Z, 2444.79–2444.85 m MDBRT). B.) An example of a clastic dyke cutting into the edge of a tuff (14/10-9Z, 2444.80–2444.85 m MDBRT). C.) A clastic sill intruding completely within a tuff representing a zone of weakness (14/10-9Z, 2451.60–2451.82 m MDBRT). D.) A clastic dyke arcing down and through a tuff, illustrating the preferential relationship between dyke emplacement and the zones of weakness (14/10-9Z, 2453.66–2453.79 m MDBRT).

199x278mm (300 x 300 DPI)

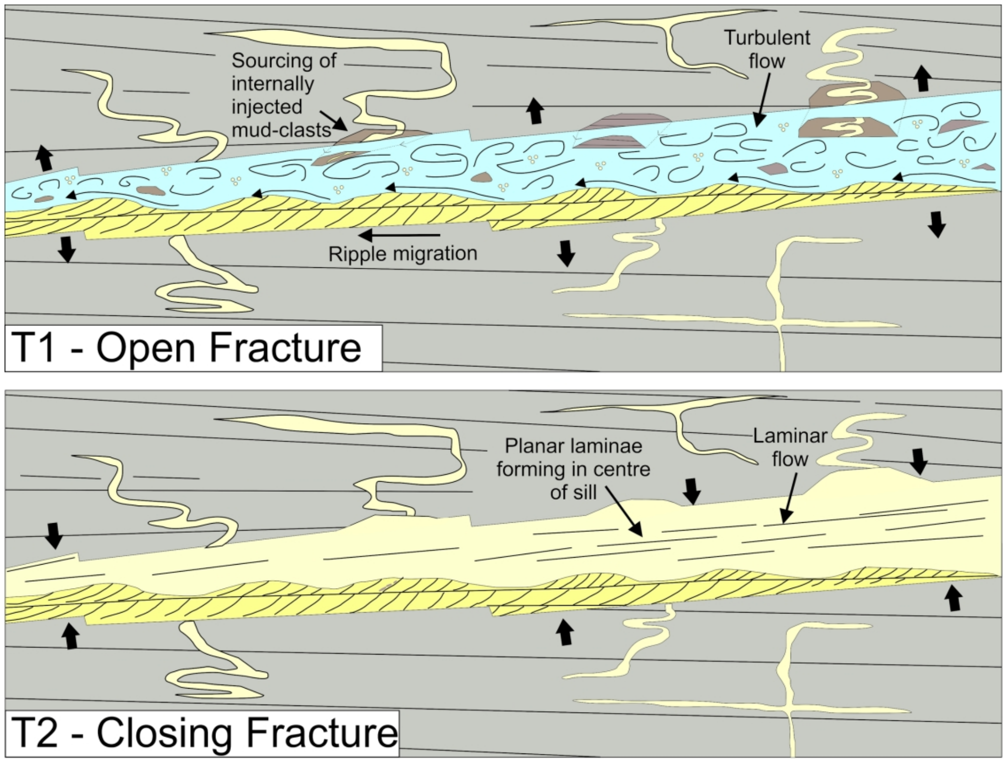

Figure 11.) A conceptual model for the infilling of clastic sills with sediment. A.) At 'T1', the ripple cross-lamination is developed during a period when the fracture is open and the sill-dyke systems are connected to the palaeo-seafloor. The migration of the ripple bedforms can only take place if the fluid concentrations were sufficiently dilute, which might imply an open fracture. Note the erosion of mud-clasts from the host rock that contain internal injectites. B.) At 'T2', the fracture is beginning to close or is about to close, with the compression resulting in an increase in sediment concentrations and the development of laminar flow. Eventually, this results in the in-situ freezing of typically structureless or planar laminated, well-sorted sand, which effectively infills the remaining space in the fracture. Commonly, this late-stage flow infills the centre of a sill, but theoretically could be found anywhere within the fracture.

204x159mm (300 x 300 DPI)

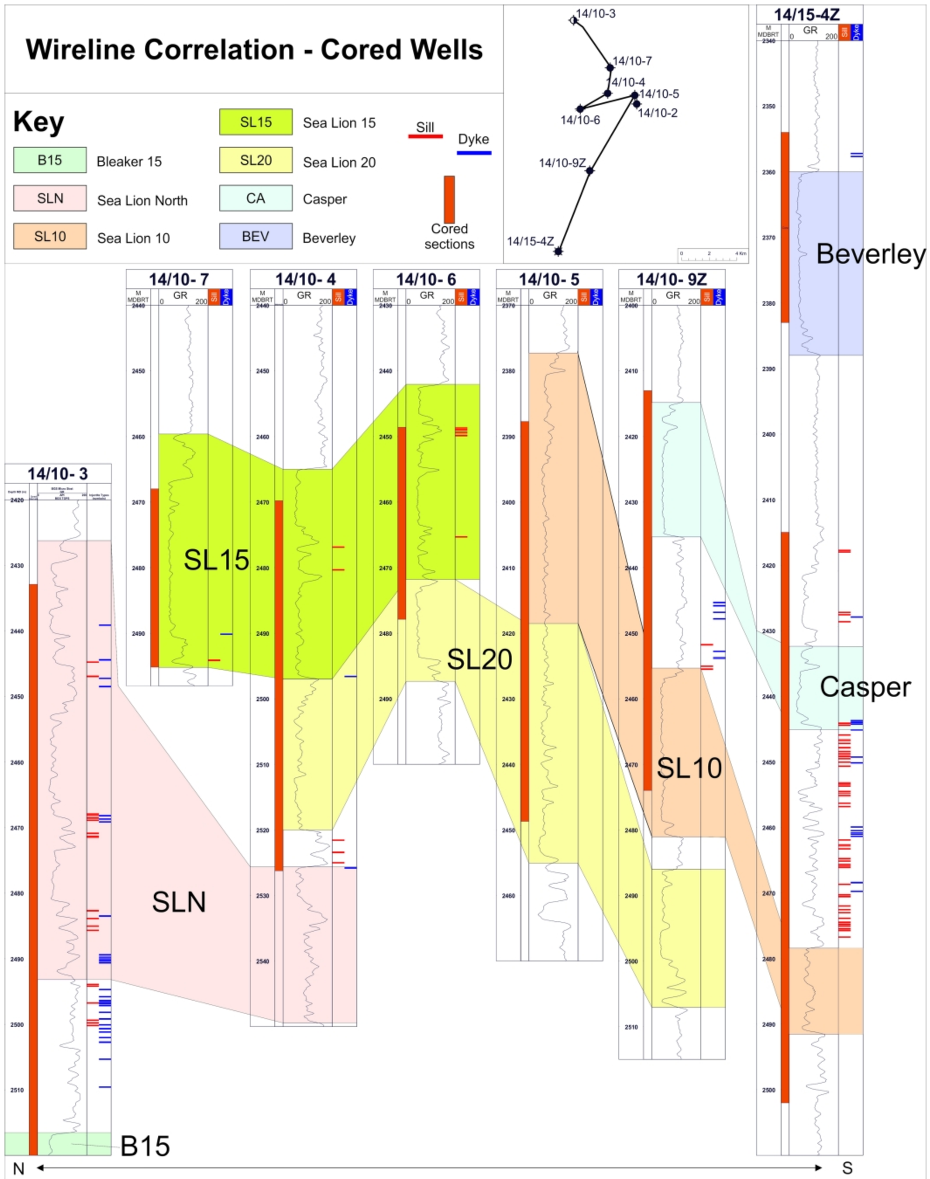

Figure 12

Figure 12.) A broadly north-south oriented (see inset) wireline correlation of cored wells. The vertical position in the well and injectite type (sill or dyke shown in red or blue, respectively) are illustrated. The injectites are distributed in four groupings: above the Bleaker 15 Fan (B15) and within/above the Sea Lion North Fan (SLN); within the Sea Lion 15 lobe (SL15) of the Sea Lion Fan; overlying the Sea Lion Fan, chiefly above the Sea Lion 10 lobe (SL10); and above/below the Casper and Beverley Fans.

286x372mm (300 x 300 DPI)

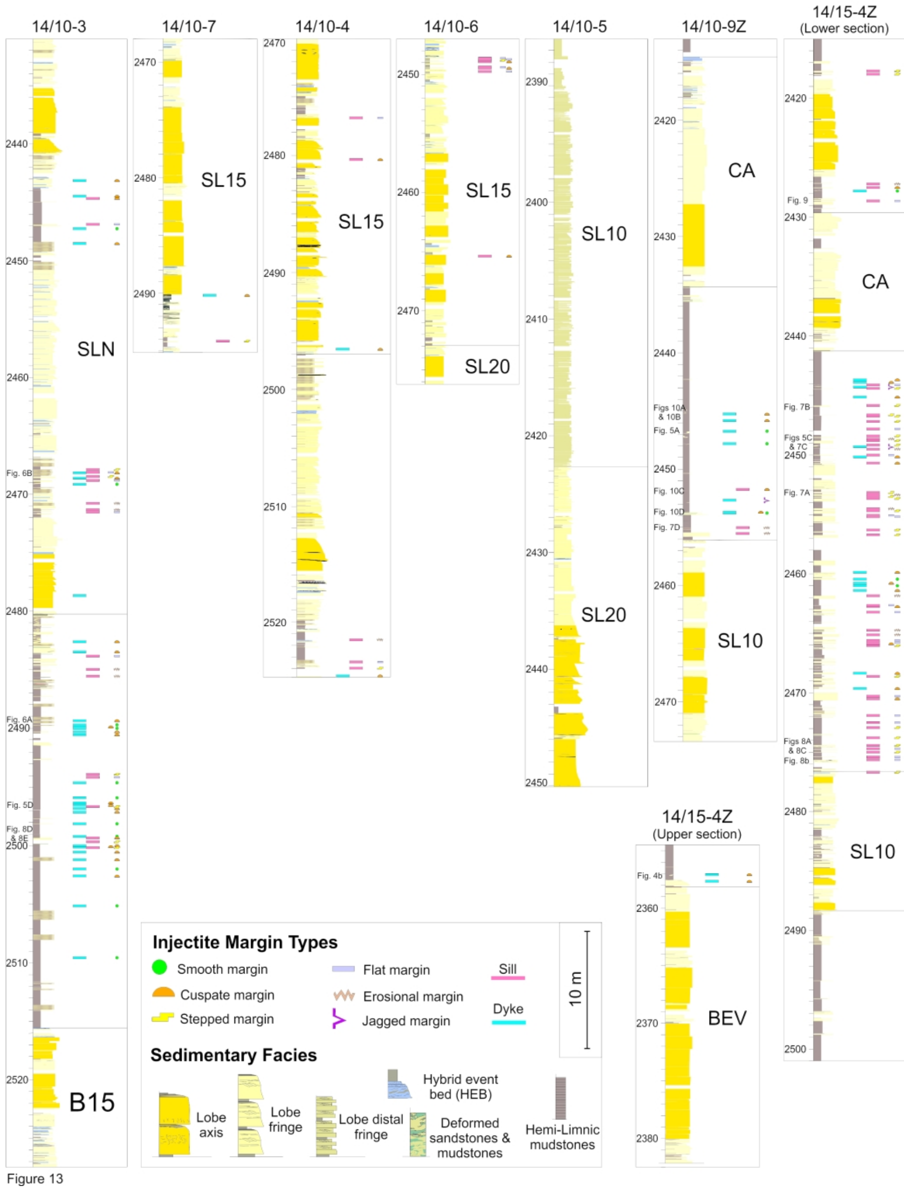

Figure 13.) Sedimentary logs of cored intervals within wells that intersect the Sea Lion North (SLN), Bleaker 15 (B15), Sea Lion (SL; 20, 15 and 20), Casper (CA), and Beverley (BEV) fans. The sedimentary logs are coloured in terms of facies associations, using the facies model set out in Dodd et al., 2019. The position of the 143 injectites has been plotted, with dyke or sill geometries recorded as a blue and red bar, respectively. Margin types, including: smooth; cuspate; stepped; flat; erosional; and jagged, have been plotted to demonstrate vertical (and in some respects lateral) distribution of injectite morphology.

286x380mm (300 x 300 DPI)

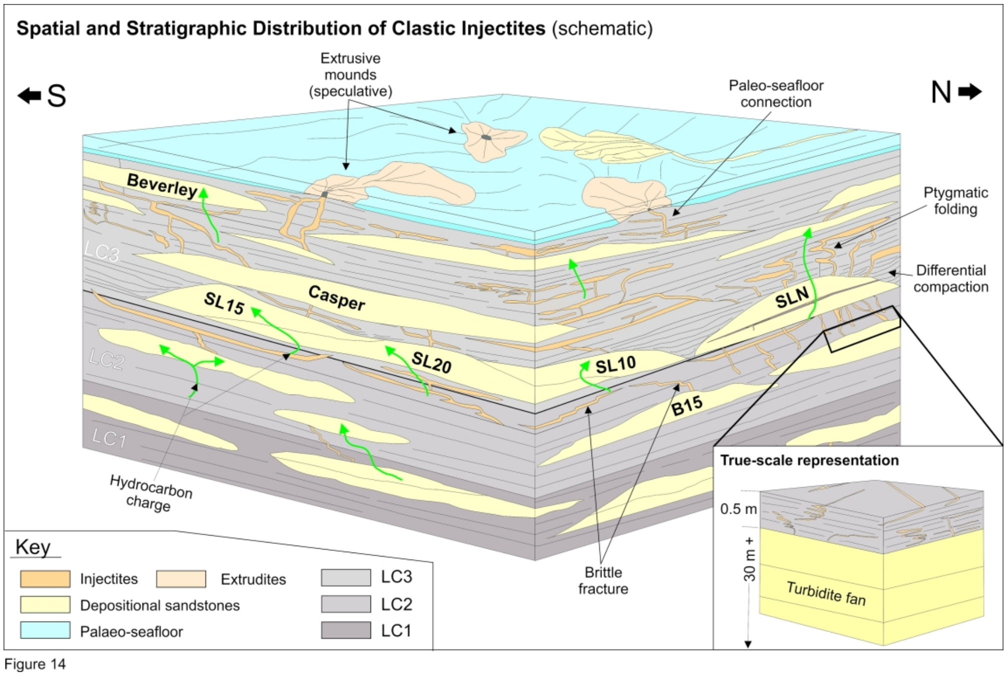

Figure 14.) A conceptual 3D block diagram (schematic), illustrating the distribution, style and geometries of injectites observed in the core data through the SLIS, and their relationship with the Bleaker 15 (B15), Sea Lion North (SLN), Sea Lion (SL20, SL15 and SL10), Casper, and Beverley fans. The injectites of the SLIS have the potential to form fluid conduits between any disconnected reservoir intervals, and may have facilitated more effective hydrocarbon migration and charge through the succession.

288x192mm (300 x 300 DPI)

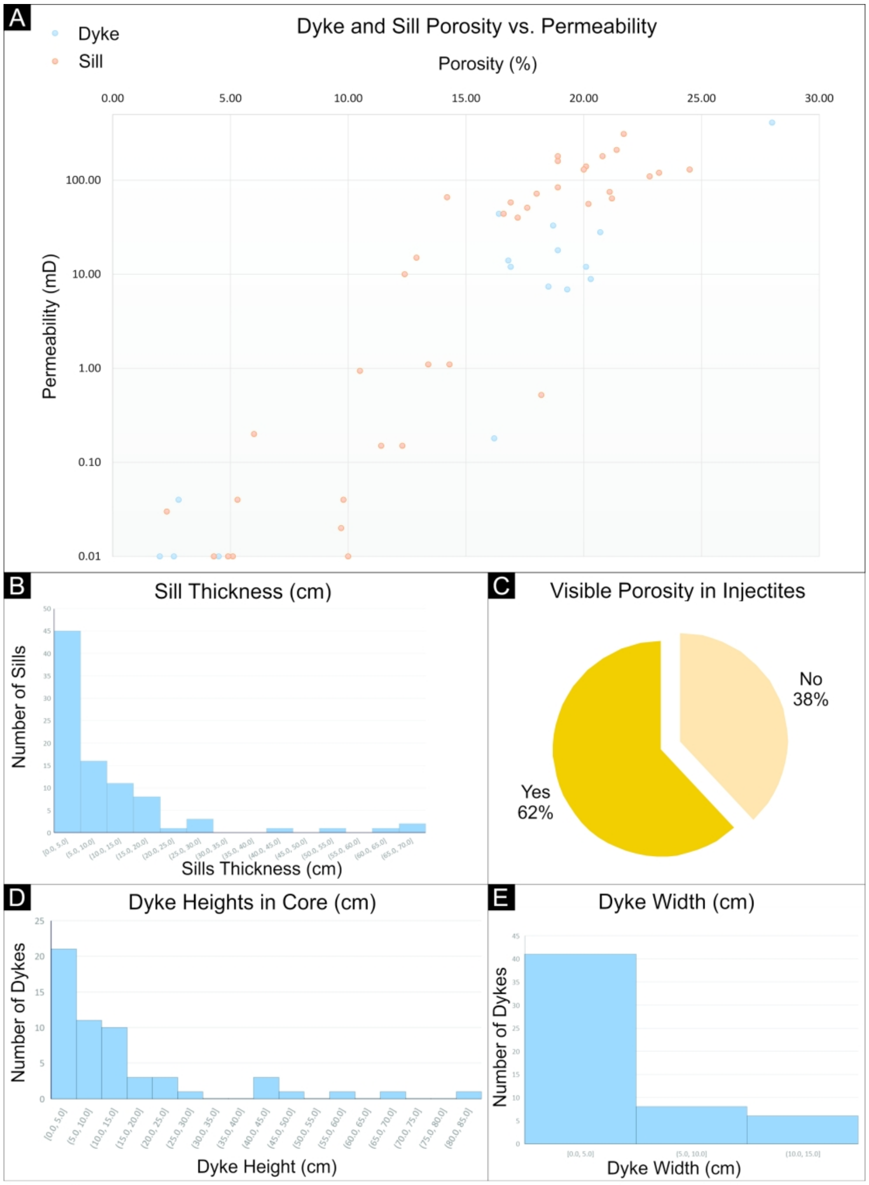

Figure 15

Figure 15.) Quantitative data from the 143 injectites of the SLIS, which could be used to populate fine-scale reservoir models that need to incorporate the potential effects of sub-seismic-scale injectites. A.) Scatter plot of core-plug porosity vs. permeability (logarithmic) from both dykes and sills. A linear trend of increasing permeability with increasing porosity is displayed. In general, sills display higher porosities and permeabilities than dykes. B.) Sill thicknesses (cm) within the SLIS. C.) Visible porosity in the injectites, observable in core data. D.) Dyke heights (cm) in core data, with most reaching up to 25 cm. E.) Dyke width (cm) observed in core data. The upper limit of dyke width is limited by the diameter of the core data (c. 12 cm).

201x280mm (300 x 300 DPI)